Reduced Thermal Modeling and Material Property Database for CubeSat Thermal Analysis

Dhrumil Patadia

Delft University of Technology

TU Delft

Reduced Thermal Modeling and Material Property Database for CubeSat Thermal Analysis

by

Dhrumil Patadia
Student Number: 6240720

for Master of Science
in Aerospace Engineering
from Delft University of Technology

Supervisor:	Dr. I. U. Balbin, TU Delft
Co-Supervisors:	Dr. S. Speretta and Dr. S. Uludag, TU Delft
Committee chair:	Dr. P. Sundaramoorthy, TU Delft
Committee external:	Dr. Y. Tang, TU Delft
Project Duration:	September 2025 – May 2026
Faculty:	Faculty of Aerospace Engineering, Delft

Cover: PICASSO CubeSat
https://www.esa.int/Enabling_Support/Space_Engineering_Technology

TU Delft

Acknowledgments

Well, I usually don't say or write a lot, but would like to say a few things about my time here at TU Delft for the last 2 years.

I am genuinely happy as I am writing this final page of my thesis. The things I have learned here in Delft, both academically and personally, have really made me a better person. I am so glad that I have made good friends whom I will cherish for life. I am grateful for all the ups and downs during this journey and would not want to change a thing.

I would like to thank my supervisors (Ines, Stefano and Sevket) who have helped me with this thesis as I have learned a lot more than I expected and also for the fact that they have been very helpful whenever I have reached out to them.

I am very grateful to Ines, as she has always pushed me to do better. Thank you for being there and motivating me, especially during the days when work was not going very good. Your excitement about the project and the technical discussions meant a lot and I am glad you were my supervisor for the last seven-eight months.

I would also like to thank Ing. B. Ibrahim from the Applied Sciences faculty for helping me with the measurements for solar absorptivity.

To all my friends who have been there for me, thank you! Without you, it would be very difficult to have spent these two years.

Finally, I would like to say thank you to my parents who have supported me, unconditionally, in every way possible.

The last thing I want to say is that this marks not an end, but a beginning. I am excited for the future and there is still much to learn, much to accomplish, and many goals I aspire to achieve, come what may.

Dhrumil Patadia
Delft, April 2026

Contents

Nomenclature

Abbreviations

Abbreviation	Definition
ADCS	Attitude Determination and Control System
Cp	Specific Heat Capacity
ECSS	European Cooperation for Space Standardization
EPS	Electrical Power System
ESA	European Space Agency
IR	Infrared
ISA	International Standard Atmosphere
MLI	Multi-Layer Insulation
PCB	Printed Circuit Board
TC	Thermocouple
TCS	Thermal Control System
UV-Vis	Ultraviolet–Visible Spectroscopy

Symbols

Symbol	Definition	Unit
A	Area	[m^2]
A_{cond}	Conduction area	[m^2]
A_{rad}	Radiating area	[m^2]
B	Radiative exchange factor	[-]
C_p	Specific heat capacity	[J/kg·K]
D	Characteristic length / diameter	[m]
E_λ	Spectral irradiance	[W/m^2·nm]
G	Conductance	[W/K]
h	Convective heat transfer coefficient	[W/m^2·K]
I	Measured intensity	[-]
I_0	Incident intensity	[-]
k	Thermal conductivity	[W/m·K]
L	Length / distance	[m]
Nu	Nusselt number	[-]
P	Power / pressure (context dependent)	[W] / [Pa]
Pr	Prandtl number	[-]
Q	Heat transfer rate	[W]
Ra	Rayleigh number	[-]
r	Reflection ratio	[-]
T	Temperature	[K]
V	Velocity	[m/s]
α	Absorptivity	[-]
α_s	Solar absorptivity	[-]
ϵ	Emissivity	[-]
ϵ_{IR}	Infrared emissivity	[-]
λ	Wavelength	[nm]
μ	Dynamic viscosity / friction coefficient	[Pa·s] / [-]

Symbol	Definition	Unit
ν	Kinematic viscosity	[m^2/s]
ρ	Density	[kg/m^3]
σ	Stefan–Boltzmann constant	[$W/m^2 \cdot K^4$]
τ	Transmittance	[-]

1

Introduction

A satellite in orbit is continuously exposed to a complex and dynamic thermal environment. Heat is received primarily from three external sources: direct solar radiation, Earth's reflected sunlight (albedo), and Earth's emitted infrared (IR) radiation. Additionally, the satellite experiences periodic transitions through eclipse zones, during which solar input is completely absent. These varying heat fluxes cause significant temperature fluctuations across the spacecraft's structure and subsystems.

To ensure that all onboard components operate within their specified temperature limits, satellites employ active and/or passive thermal control systems. For CubeSats and other small satellites, maintaining thermal balance is particularly challenging due to their compact size, limited surface area for radiators, and power constraints that restrict the use of active control methods like heaters or pumps. As a result, thermal control for CubeSats relies heavily on careful design and material selection during the early stages of development.

However, detailed thermal analysis such as that performed using professional tools like ESATAN-TMS, SINDA/FLUINT, or Thermal Desktop requires considerable time, expertise, and computational resources. Small satellite teams, often composed of students or small research groups, tend to prioritize mission functionality and payload development over detailed thermal modeling, since it is not their primary mission objective. Moreover, the design of small satellites evolves through multiple iterations, and performing a complete thermal analysis or experimental validation after every modification becomes impractical. This iterative neglect can result in inadequate thermal management, leading to localized subsystem overheating, component degradation, or even complete mission failure.

Another significant challenge is the inconsistency and uncertainty in the optical and thermal properties (such as absorptivity, emissivity, and contact conductance) of materials and surface coatings used in spacecraft. Values reported in literature and online databases can vary widely due to differences in surface preparation, aging effects, and measurement conditions. This lack of reliable property data introduces errors into thermal models and reduces the accuracy of predictions made during preliminary design stages.

To address these issues, this thesis focuses on two key aspects aimed at improving preliminary thermal analysis for CubeSats and small satellites:

- Development of a comprehensive database through testing of optical and thermal properties for materials commonly used in small satellite structures.
- Creation and validation of reduced thermal models for typical spacecraft components such as printed circuit boards (PCBs). These simplified models can be used early in the design process to approximate temperature distributions while significantly reducing computational time and complexity.

Together, these two developments aim to provide small satellite teams with practical tools that improve thermal design confidence during preliminary stages, helping to identify potential thermal risks early and minimize the chances of mission failure due to inadequate thermal control.

1.1. Literature Review

This section highlights the lack of thermal analysis performed by student teams and the issues related to it. Further, the various procedures for measurement of thermo-optical properties are given along with the current work on reduced thermal models that can be used for quick iterative thermal analysis. This will later help build a methodology that can help attain the research objective outlined in the next chapter.

Cubesats in general have short development times and this often leads to lack of thermal control solutions[1]. Further, student teams often have a low budget, less expertise and no access to a vacuum chamber which makes it difficult to perform thermal analysis or carry out thermal balance tests[2]. In addition to this, the unreliable thermo-optical properties used, as manufacturers do not provide these values, leads to high uncertainties in temperatures obtained from any preliminary thermal analysis.

Delfi-PQ, developed by TU Delft, experienced ”unforseen problems”[3] which led the electrical power sub system to operate from -10°C to 25°C, instead of the planned range of 5°C to 40°C.

The student team at TU Darmstadt could not perform a proper thermal analysis due to software licensing issues and had to rely on a MATLAB code available which imposed certain limitations on the way the configuration can be defined and the lack of attitude modification of the satellite [4].

Another discussion[5], highlights how CubeSats are built using components off the shelf and that thermal control engineering is overlooked due to the time required and its complexity.
All these examples indicate the issues highlighted earlier.

In thermal analysis of a CubeSat, parameters like the optical properties of external surfaces, orbital parameters and contact conductance play a critical role in determining the spacecraft's temperature distribution and thermal balance. Parameters such as solar absorptivity (α) and infrared emissivity (ϵ) define how much solar radiation is absorbed and how effectively heat is radiated to space. The ratio $\frac{\alpha}{\epsilon}$ largely governs the equilibrium temperature of the satellite's surfaces. To ensure stable operation of onboard electronics and payloads, material coatings and surface finishes must be carefully selected based on the expected orbital environment, attitude, and exposure to the Sun and deep space. The temperature values are the most sensitive to changes in optical properties of components facing solar heat flux and values of contact conductance[6][7], thus getting accurate values is very important for the thermal design.

The sensitivity analysis performed by F.S. Meijering[7] indicates that a 10% change in the absorptivity leads to a 6.6°C change in maximum temperature. He also showed that a 10% change in the rotational rate can cause a 5.3°C change in maximum temperature.

The sensitivity analysis conducted for Delfi-PQ [8] shows that variations in the optical properties of the external surfaces can lead to temperature changes up to three times larger than variations in the optical properties of interior surfaces and components. Additionally, the emissivity of internal surfaces was found to influence the minimum battery temperature to approximately half the extent of the external surface optical properties. Given that Delfi-PQ experienced a 15°C deviation in the expected temperature of the EPS unit, these findings suggest that both external and internal optical properties can significantly influence thermal predictions and should therefore be carefully considered in thermal modeling.

1.1.1. Thermo-optical property Data available in literature

Data from literature is provided for components like PCBs, solar cells and solar panels in table 1.1. The components have been chosen on the basis of components to be used in Delft-twin and the Da Vinci satellites.

Table 1.1: Thermo-optical properties of CubeSat components

Component	Property	Value	Reference
PCB (2 copper layers)	k (W/mK)	17.7	[9]
	C_p (J/kgK)	589	[8]
	ε	0.8 to 0.91	[10][11][12]
Solar Panel (White Coating)	k (W/mK)	30	[9]
	C_p (J/kgK)	589	[8]
	ε	close to unity	[13]
	α_s	0.21	[13]
Solar Panel (Black Coating)	k (W/mK)	30	[9]
	C_p (J/kgK)	589	[8]
	ε	close to unity	[13]
	α_s	0.94	[13]
Solar Cells	ε	$>$0.86	[14]
	α_s	$<$0.91	[15]

While literature provides a reference for thermo-optical values, the sensitivity of CubeSat temperatures to external surface properties, combined with observed discrepancies in flight missions such as Delfi-PQ, indicates that property assumptions need to be validated. Therefore, experimental validation of thermo-optical properties for commonly used CubeSat components is necessary. Such a validated database would help develop reduced-order thermal models that can be used to provide reliable first-order temperature estimates during initial design phases.

1.1.2. Thermal Balance Tests

Thermal Balance Tests are carried out as part of the subsystem Thermal Vacuum Test and include specific hot and cold phases that replicate the most extreme flight conditions. These tests take place in a controlled environment with predefined operational parameters to simulate the worst-case flight scenarios. During each phase, the subsystem is allowed to thermally stabilize until steady-state temperatures are achieved. Typically, a thermal balance test consists of three phases: a hot operational phase and a cold operational phase, which verify the subsystem's operational thermal limits, and a cold non-operational phase, which demonstrates the non-operational limits and assesses the performance of the heater system. These tests can take up to a day for very sophisticated systems and drive up costs significantly. The temperatures at various locations measured in these tests are correlated with the thermal mathematical models and strict guidelines set by ECSS[16] are followed which require internal temperatures to be within 5K and external tmperatures within 10K with a mean deviation of $\pm$2K.

These tests can also be be done on a smaller scale, for example, for a PCB instead of the entire cubesat in order to determine specific property values (infra-red emissivity, heat capacity or thermal conductivity) when only one is unknown.

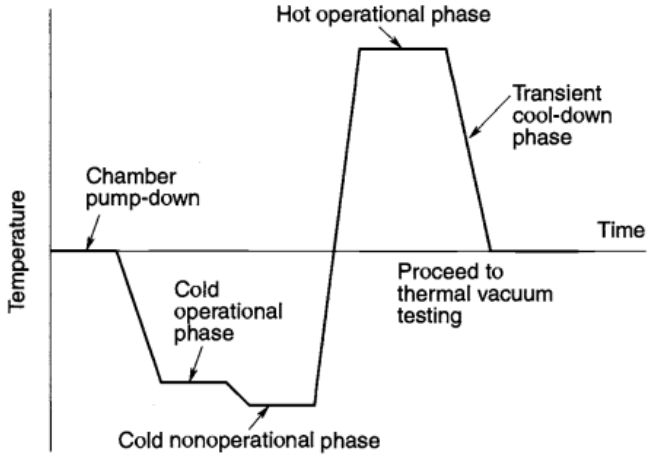

Figure 1.1: Simple thermal balance test profile
[17]

1.1.3. Contact Conductance

When we look at heat transfer in a satellite, an important aspect is the thermal contact conductance between two surfaces in contact with each other. While dealing with cubesats built by student teams, the major contact conductance considerations are in the spacer-PCB stack. It is defined as:

$$h_c = \frac{q}{\Delta T}$$

where, q is the heat flow across the interface and ΔT is the temperature drop. The modes of heat transfer could be conduction, convection and/or radiation. But for applications in space, convection and radiation can be neglected between contact surfaces[18].

The exact determination of contact conductance based on empirical relations is very complex as it depends on various factors like surface roughness, contact pressure, hardness, thermal conductivity, and gap thickness.

Testing of contact conductance for spacers is usually done by bringing two cylinders in contact under an axial load inside a vacuum jar[19]. Thermocouples are placed along the cylinder surface to determine the heat flow. Based on the known thermal conductivity of the cylinder, the contact area and the heat flow, the contact conductance can be determined[20].

Philipp B. Hager et al.[21] setup an thermal balance test experiment to measure contact conductance values for spacers in cubesats. This included placement of a spacer-washer stack between an aluminum plate and a copper plate. The overall linear conductance was measured for the spacer-washer stack. Further, values of multiple empirical relations were compared with experimental results and maximum errors of 20$\%$ have been reported. This deviation from empirical relations is significant and thus the author suggests that one can use the experimental values presented in this paper as a baseline for initial thermal design.

Furthermore, Matteo Quirino et al. [22] used the thermal contact conductance values reported by Philipp B. Hager et al. [21] for their model correlation. However, these values did not align with the ECSS standards [16]; instead, a value approximately 41$\%$ of the original had to be applied to achieve agreement with the standards.

Empirical relations have been developed by Yovanovich et al.[23], a few of them consider elastic deformation while some consider plastic deformation. They all require some basic computations that involve calculation of the effective thermal conductivity, surface roughness, and asperity slope. The

most common model used is the Cooper–Mikic–Yovanovich (CMY) model[24]:

$$\frac{h_c}{k_s}\frac{\sigma}{m} = a_1 \left(\frac{P}{H_c}\right)^{b_1}$$

where
a_1 = 1.45 and b_1 = 0.985,
h_c = thermal contact conductance [W·m^{-2}·K^{-1}],
k_s = effective thermal conductivity of the two materials in contact [W·m^{-1}·K^{-1}],
σ = root-mean-square (RMS) surface roughness [m],
m = mean absolute slope of surface asperities [-],
P = contact pressure [Pa],
H_c = micro-hardness of the softer material [Pa].

The European Space Agency has a method where it calculates the contact conductance at a joint interface by referring to a database [25] of contact conductance values that varies with materials, surface finish and contact pressure. With reference to spacers in cubesats, they propose a method to determine the axial force based on applied torque. The calculation for axial force is given as:

$$\tau_{\text{tot}} = F_{\text{ax}}\left(0.16P + 0.58\mu d_2 + \mu_b r_m\right)$$

where
τ_{tot} = total tightening torque [N·m],
F_{ax} = axial (preload) force in the bolt [N],
P = thread pitch [m],
μ = coefficient of friction in the threads [-],
d_2 = pitch diameter of the bolt [m],
μ_b = coefficient of friction under the bolt head or nut face [-],
r_m = effective friction radius under the head or nut [m].

Considering the variation in contact conductance values as highlighted by Philipp[21] and Matteo[22], the linear conductance across the spacer-PCB stacks need to be experimentally determined as a function of the torque applied.

1.1.4. Reduced Modeling

Reduced model refers to a model of a component with a minimum number of nodes for thermal simulations in order to reduce simulation complexity. The work by Brouwer et al.[1]suggests a set of steps to make a reduced model.

- Identify a submodel like a structural element, PCB or a panel.
- Identify thermally relevant parts on the submodel based on power dissipation, thermal conductivity, heat capacity and thermal connections as shown in figure 1.2
- Next is comparison of the ESATAN simulations of the reduced sub-model with actual test of the component.

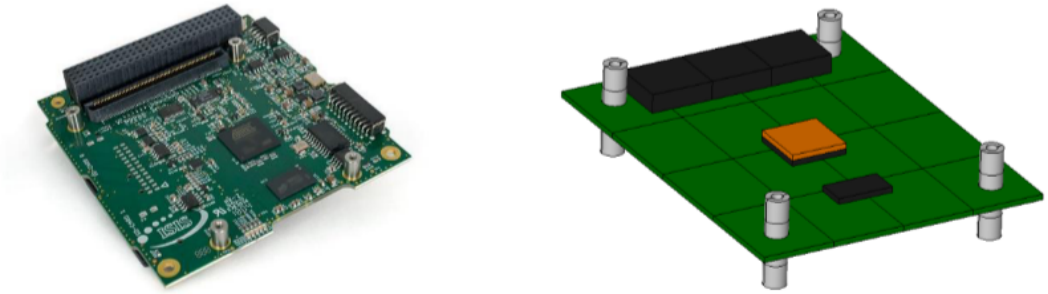

Figure 1.2: Reduced model of an on board computer
[1]

The authors also performed their own set of tests[26] and found an accuracy of 10K which they mentioned was low and suggested the improvement of their initial ESATAN models and again perform correlations.

Further, extensive work has been done by Thales Alenia Space and ASTRIUM where they managed to reduce the number of nodes, for their 4000C4 Telecom spacecraft from 2873 to 323. But their work mentions the use of reduction modules that are internal and not published in literature.

1.1.5. Optical Property Measurement

In thermal analysis of a CubeSat, the optical properties of external surfaces play a critical role in determining the spacecraft's temperature distribution and thermal balance. Parameters such as solar absorptivity (α) and infrared emissivity (ϵ) define how much solar radiation is absorbed and how effectively heat is radiated to space. The ratio $\frac{\alpha}{\epsilon}$ largely governs the equilibrium temperature of the satellite's surfaces. To ensure stable operation of onboard electronics and payloads, material coatings and surface finishes must be carefully selected based on the expected orbital environment, attitude, and exposure to the Sun and deep space. The temperature values are the most sensitive to changes in optical properties of components facing solar heat flux and values of contact conductance[6][7], thus getting accurate values is very important for the thermal design.

Solar absorptivity, as a function of wavelength and temperature, is often calculated from the measurement of reflectivity and transmission[27][28].

$$\alpha(T, \lambda) = 1 - \rho(T, \lambda) - \tau(T, \lambda) \tag{1.1}$$

where:

$\alpha(T, \lambda)$: absorptance
$\rho(T, \lambda)$: reflectance
$\tau(T, \lambda)$: transmittance

Usually, the sample is opaque and τ can be considered zero.

Emissivity of a surface is required in the Mid-Infrared spectrum (4000 to 400cm^{-1}) because this corresponds to temperatures of 100K to 1200K which is where our spacecraft temperatures will lie within.

The European Space Agency highlights the following methods for measurement of solar absorptivity [28]. The first method uses an integrating sphere, shown in figure 1.3, where the total specular and diffuse reflection can be measured. The basic principle of an integrating sphere is that light reflected off of a sample is allowed to fall on a sphere which has a lambertian surface (diffuse reflection) and this leads to uniform distribution of the energy over the inner surface of the sphere. A detector placed on one section of the sphere measures some energy which will be proportional to its area with respect to that

of the sphere. This data can be used to obtain the absorptivity based on a simple energy conservation using equation 1.1.

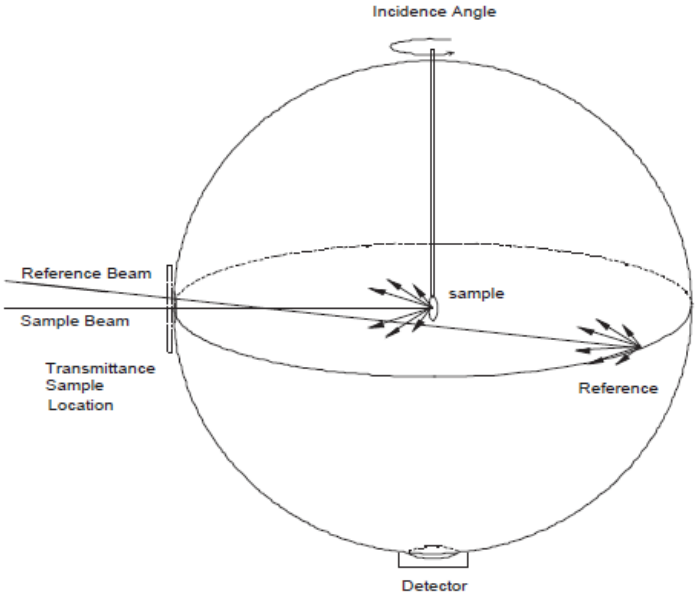

Figure 1.3: Integrating sphere
[27]

Second, is a comparative test method where the reflection of a Xenon flash by a known material is compared to that of an unknown material. The disadvantage is that this works only for opaque flat samples and also has a spectrum that is slightly different from the solar spectrum.

There are various methods for measurement of emissivity. First, is the use of a infrared reflectometer [27] which is a device that consists of 2 rotating cavities, one of which is heated and other is at room temperature. The sample is alternately irradiated by the hot and cold cavities and the reflected energy from the sample is measured by a detector. The only limitations are that the sample must behave like a grey body and the reflection must be lambertian (does not vary with angle of incidence).

Second, is the the use of an integrating sphere with a IR reflectometer. The reflection is measured and the absorptance obtained is integrated to obtain the total emissivity (grey body assumption).

$$\varepsilon = \frac{\int A(\lambda)E(\lambda)\,d\lambda}{\int E(\lambda)\,d\lambda}$$

where,
$A(\lambda)$ is the spectral absorptance,
$E(\lambda)$ is the spectral blackbody emission spectrum, and
ε is the total hemispherical emissivity.

Various sources[29][30][31][32] discuss the use of an infrared camera to measure the radiation from the sample. The work by Orlove[30] discusses a concept called emissivity calibration which measures radiation from a sample at two different temperatures other than the ambient temperature and then uses the data to eliminate the background radiation. The drawback is the assumption of constant emissivity over the temperature range. Vellvehi et al.[32] initially discusses the classical approaches like using coatings of known emissivity or comparison of two infrared images and linearization of the black body radiation dependence on temperature. The author then proposes a better approach which considers

a linear relationship between observed heat fluxes which leads to the measurement to be improved to within 1°C while the previous methods had an error of at least 4°C. The only limitation is that calibration parameters of the camera must be known or should be determined using a blackbody reference. Also, the emissivity and environmental heat flux is considered constant throughout the temperature range.

Further, Gabriella R. et al.[33] measured optical reflectance and transmittance using UV-Vis-NIR spectrophotometer using a double beam Perkin Elmer mod. 1050+ instrument, equipped with 15cm diameter integrating sphere. Also, IR reflectivity was measured using Invenio-x: an instrument by BRUKER which also uses an integrating sphere. The figures 1.4 & 1.5 given below indicate the choice of sources and detectors used for these instruments based on the wavelength range. The source for the UV-Vis-NIR is Deuterium and Tungsten lamps while for the mid-infrared the source is a silicon carbide globar light source. The detectors are indium-gallium-arsenic and liquid nitrogen-cooled mercury cadmium telluride (LN2-MCT) respectively.

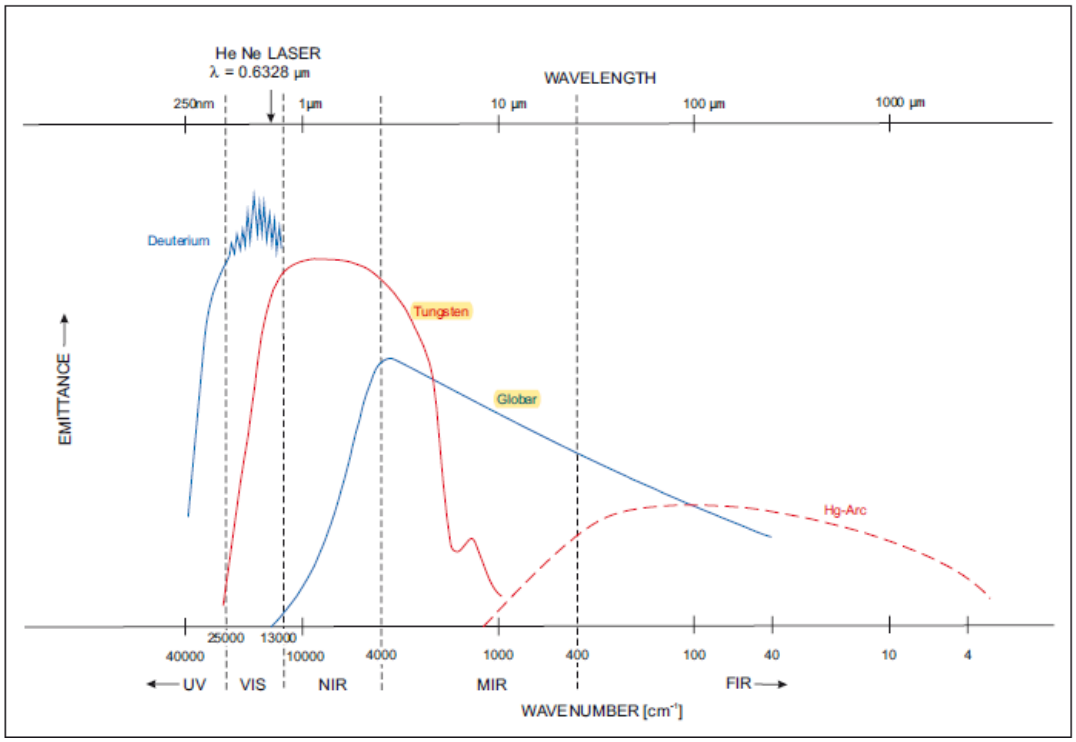

Figure 1.4: Radiation sources selected according to the relevant wavelength range [34]

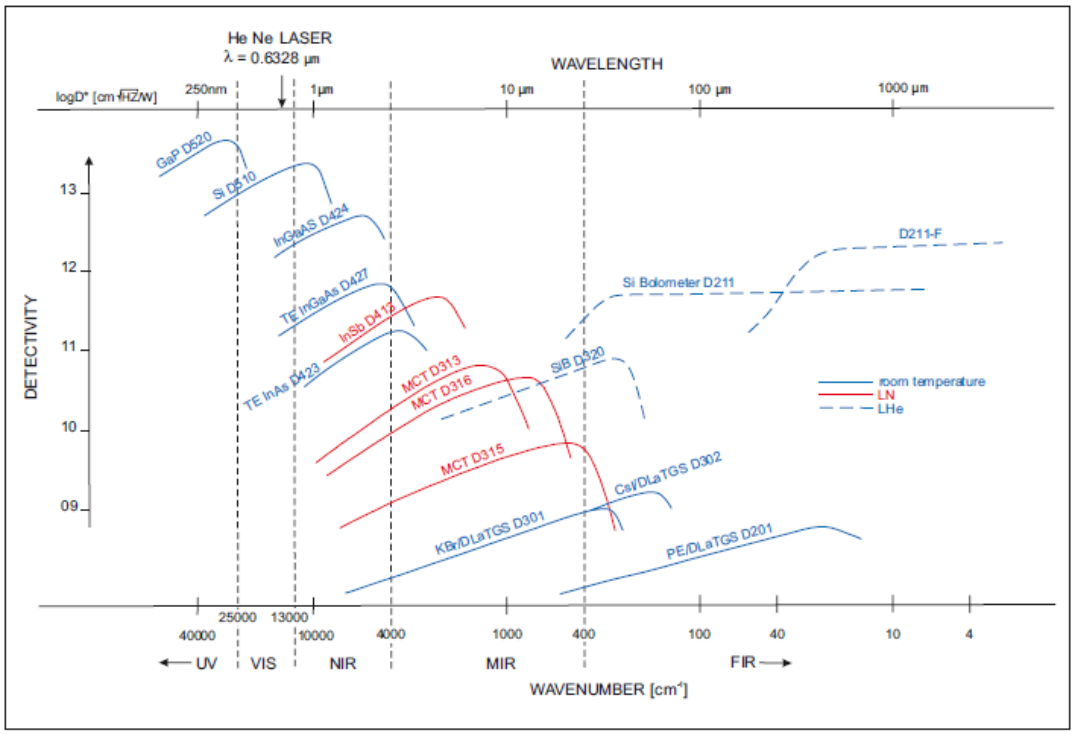

Figure 1.5: Detectors selected according to the relevant wavelength range [34]

1.2. Research Objective and Research Question

The literature review reveals uncertainties in the thermo-optical properties available and also the need to develop reduced-order models that can improve temperature estimations in the initial thermal analysis performed by smallsat teams. To address this gap, the research question is formulated as follows:

How can an integrated framework, that combines experimental determination of thermo-optical properties with reduced-order thermal modeling, be developed to quantify the accuracy of preliminary thermal modeling for small satellite teams?

This can be broken down into the following sub-questions:

1. How can experimentally obtained thermo-optical property data be compiled into a reliable database for CubeSat materials?
2. How can reduced-order thermal models be generated by using the database?
3. How can the reduced-order thermal sub-models be compared to experimental data?

1.3. Research Plan

To answer **sub-question 1**, conductance test, thermal balance test and FTIR and UV/Vis will be conducted.

Regarding the **conductance test**, the linear conductance across the PCB-spacer stack will be calculated by placing the stack, covered in MLI, inside a vacuum chamber. The PCBs will be heated using in-built heaters and temperatures will be measured at various locations using thermocouples and inbuilt temperature sensors on the PCBs. Further, the temperature data during steady state will be used to determine the linear conductance across the PCB-spacer-PCB stack. This includes the combined effect of connectors, through conductance across the spacer and contact conductance at the PCB-spacer interface. This will be performed across a range of torque values.

For the **solar absorptance** tests, the cleaned samples of the solar cells and panels will be placed in a UV-Vis spectrometer with an integrating sphere, which collects both specular and diffuse reflection. This is converted to a reading of the total hemispherical absorptivity. Measurements will be conducted over the full solar spectrum.

For **IR emissivity** and **thermal conductivity**, thermal balance tests will be carried out in a vacuum chamber. The sample will be heated using kapton or calyborn heaters. The vacuum chamber will ensure convection can be neglected. Other heat loss paths through conduction and radiation will have to be accounted for. Thermocouples will be used to measure temperature drops across a path and thermal properties will be obtained using steady state heat balance.

For **heat capacity**, the sample will be heated and then allowed to cool to the environment temperature inside the vacuum chamber. The time taken for this will be noted. Further, a code will be written to model this behavior and the time taken to reach room temperature will be calculated for different values of heat capacity. The values from the code and test will be compared and the heat capacity value can be determined such that the time difference between the test and code values is minimum.

To answer **sub-question 2**, reduced thermal models of PCBs and PCB–spacer stacks will be developed to predict heat transfer between adjacent PCBs. The goal is to capture the thermal interaction between PCBs that are separated by spacers and connected through a connector, with emphasis on both conductive and radiative heat transfer paths. At the end, a temperature distribution along the surface of both PCBs will be obtained for a given power input.

It is important to note that this is for the specific case of a stack contained within an enclosure which is being used for thermal balance tests.

This will be done by first performing experiments to obtain the relevant thermal properties, such as effective conductance across spacers. Also, the effect of torque on the linear conductance across spacers will be studied. These properties, along with thermo-optical properties obtained for PCBs will then be used as input for modeling the setup in ESATAN, where reduced-order thermal models of the system will be created.

A simpler calculator will also be developed, which can make temperature estimates of the surface of PCBs without the use of ESATAN.

To answer **sub-question 3**, the reduced thermal models created in ESATAN will be compared with data obtained from thermal balance tests that will be performed in a vacuum environment. Thermocouples will be placed over both PCBs of the stack and heat will be provided to one of the PCBs via an in-built heater. The steady state temperatures of the thermal balance test will be compared with results from ESATAN and the calculator. The deviation of temperatures compared to the experimental results will be highlighted to discuss the accuracy of the model.

1.4. Report Outline

The structure of the report is as follows. **Chapter 2** describes the modeling procedure to replicate Delfi-PQ in ESATAN. It will help us determine the property values that need to be experimentally determined. **Chapter 3** describes the design of experiments for various components like solar cells, panels and PCBs. It highlights the equipment required for the tests and concludes with a database of thermo-optical properties obtained for above-mentioned components. **Chapter 4** discusses a sensitivity study performed on thermal model discussed in **Chapter 2** using property values obtained in **Chapter 3**. It gives an understanding of the deviations in temperature bounds of critical components like the battery stemming from the uncertainty in the property values obtained. **Chapter 5** discusses the calculation for linear conductance across a PCB-spacer stack with the connector involved. Further, an approach for creating a reduced model for the stack is described and validated with experimental results. Finally, in **Chapter 6** a conclusion of the work, highlighting the material property database and reduced model is given. This is followed by suggestions for future work.

2

Satellite Modeling

Delfi-PQ is a PocketQube developed by the Delft University of Technology which was launched in January 2022. It is eight times smaller than its predecessors: Delfi-C3 and Delfi-n3Xt.
The mission of Delfi-PQ was to demonstrate a reliable core bus and outer structure for a three-unit PocketQube.

Figure 2.1: Delfi-PQ

To identify the key thermal property values required for a small satellite, a thermal model of Delfi-PQ was developed.
Therefore, this chapter describes the thermal modeling procedure for Delfi-PQ by highlighting the values that need to be experimentally determined.

2.1. Properties of the model

The epoch was set to 13th January, 2022. The satellite was initially set to point with the top panel facing away from the Earth. And a constant spin of 10°/s was provided along the vector [1,1,1] in the body frame of the PocketCube in order to replicate tumbling.

Orbital Element	Value
Eccentricity (e)	0.00118
Semi-major axis (a)	6903 km
Inclination (i)	97.4°
Right Ascension of the Ascending Node (Ω)	91.85°
Argument of Periapsis (ω)	282.166°

Table 2.1: Orbital elements of Delfi-PQ

To model the heat dissipation from the internal components, three non-geometric thermal nodes were assigned to the battery, ADCS PCB and antenna PCB. The nominal case of power distribution[8] has been considered for the above mentioned boards and approximately 20% of the power is assumed as heat loss from the nodes. The heat loss has been summarized in table 2.2.

Component	Heat Loss [mW]
EPS	4.6
ADCS	2.8
Radio	2500
Battery Cell	10
Battery PCB	2.8

Table 2.2: Heat loss of spacecraft components

The geometry of Delfi-PQ has been replicated from Standardized Thermal Control Solutions for PocketQubes[8].

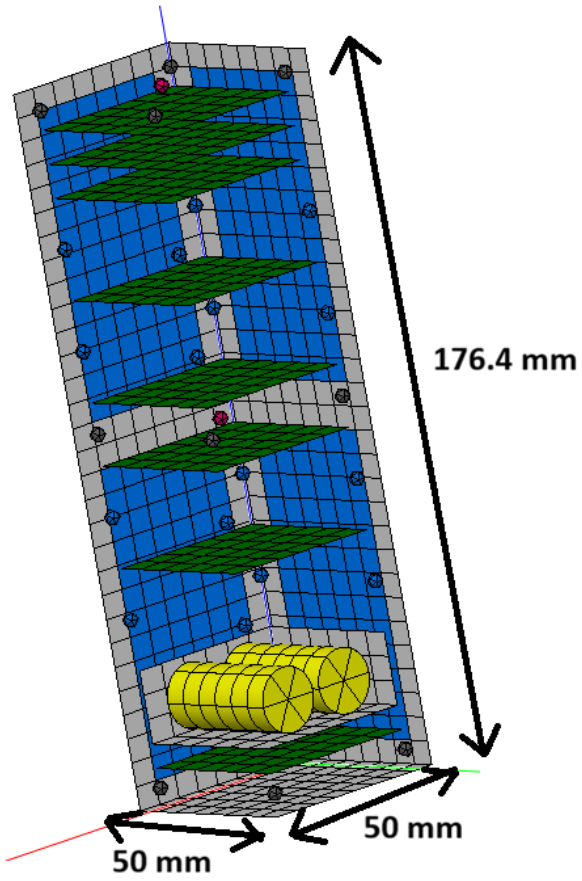

Figure 2.2: Discretised geometry of Delfi-PQ

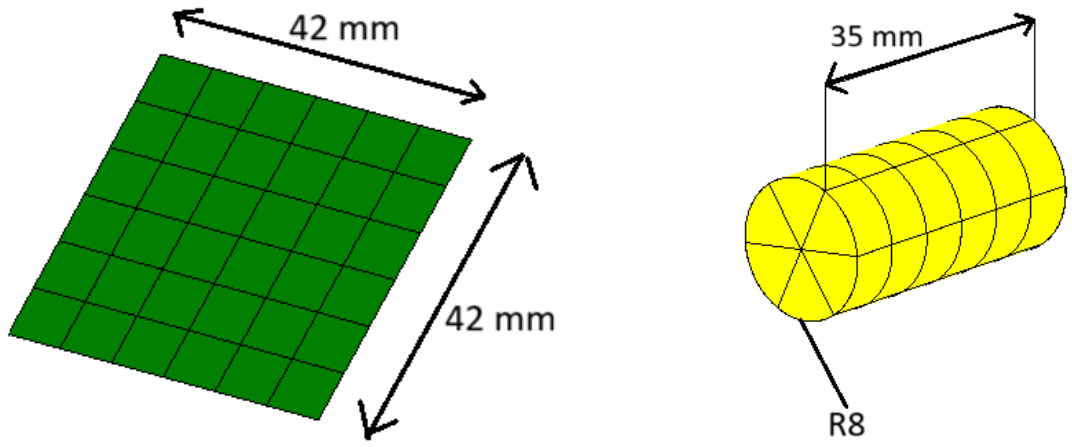

(a) PCB dimensions

(b) Battery dimensions

Figure 2.3: Component dimensions

The solar panels, solar cells and PCBs are modeled as rectangular shells. While the batteries are represented as a solid cylinder. And the spacers and standoffs are non-geometric thermal nodes.

There are 9 PCBs, 12 standoffs, 16 spacers, 2 battery cells, 8 solar cells and 6 solar panels. Notably, the top and bottom panels of Delfi-PQ are modeled as PCBs rather than panel elements. This is important to account for as the top and bottom panel get heat flux from the environment and the heat capacity difference between a panel and PCB will give different temperature extremes in orbit. There is also a plastic casing around the battery.

- The dimensions of the PocketCube are 176 mm $\times$ 50 mm $\times$ 50 mm
- Each PCB has a dimension of 42 mm $\times$ 42 mm.
- The radius of the battery is 8 mm and the length is 35 mm. The plastic casing surrounding the battery cells have the dimensions: 42 mm $\times$ 42 mm $\times$ 18 mm.

The components mentioned above need to be assigned bulk and optical properties:

- thermal conductivity
- heat capacity
- density
- infrared emissivity
- solar absorptivity

The above mentioned properties need to be determined either from literature or experimental work. As discussed in the literature review section, the uncertainties in the above mentioned properties need to be addressed.

Given the time and components available for this thesis, it was decided to **perform experiments** to determine the property values for **PCBs, solar panels and solar cells** considering they are the most commonly used components.

The values of material properties for the battery, contact conductance between the panels and cells and contact conductance of the plastic case around the battery was obtained from Standardized Thermal Control Solutions for PocketQubes [8]. This is shown in table 2.3 and 2.4

Component	Density (kg/m^3)	C_p (J/kg·K)	$k_{\text{in-plane}}$ (W/m·K)	$k_{\text{across-plane}}$ (W/m·K)	Emissivity (-)
Battery	2416	930	28	3.4	0.85
Plastic	1200	1200	0.2	0.2	0.92

Table 2.3: Material properties of components including emissivity

Component 1	Component 2	Contact Conductance (W/m^2·K)
Panel	Panel	1000
Plastic Case	PCB_Battery	4000
Plastic Case	Plastic Case	Fused

Table 2.4: Contact conductance values between components

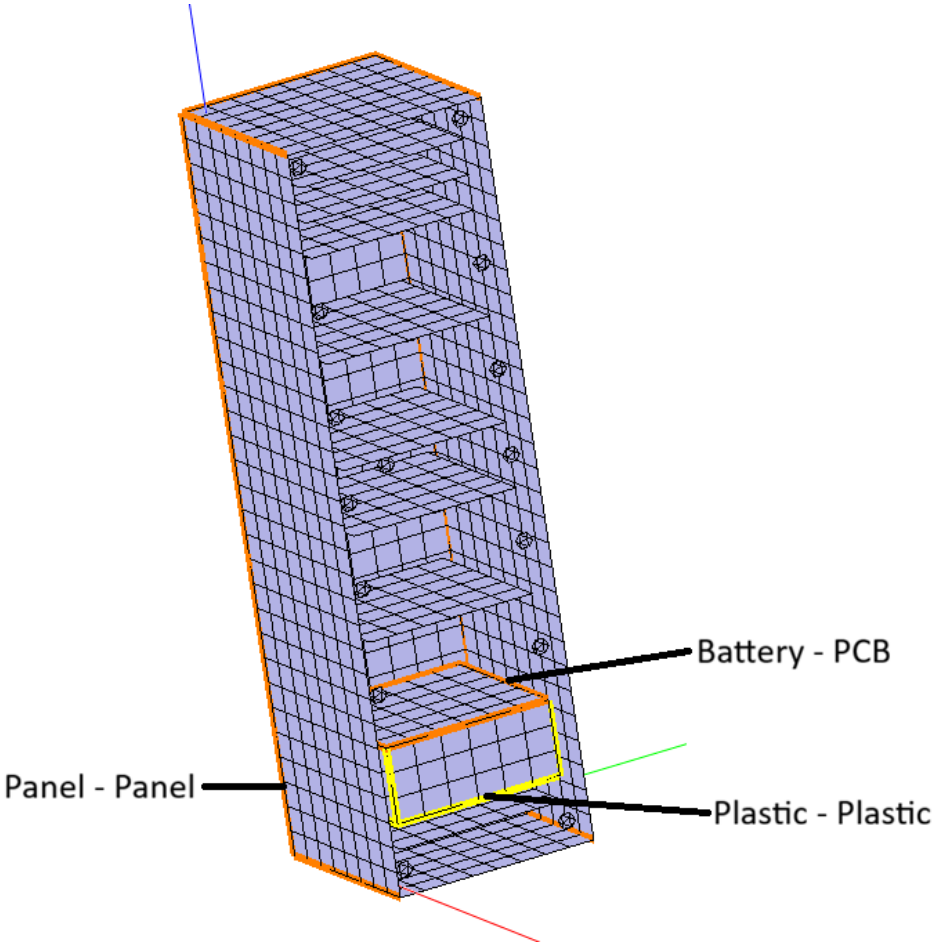

Figure 2.4: Contact Conductance locations

3

Design of experiments

As discussed in the previous chapter, thermal modeling of a small satellite requires several properties, including solar absorptivity of solar cells and panels, infrared emissivity of solar cells, panels and PCBs, thermal conductivity and heat capacity of solar panels and PCBs and the conductance across a PCB-spacer-PCB stack. This chapter describes the experimental design used to determine the desired thermal (k & C_P) and optical properties (α_s & ϵ_{IR}). A brief overview of the experiments, components, and equipment is first provided, followed by detailed descriptions of the instrumentation, test procedures, and results. **All components used in experiments have been labeled with their image and shown in Appendix E for future use, if needed**.

List of Components

- Solar Panel (150mm × 50mm)
- Solar Cell (40mm × 80mm)
- PCB (47mm × 47mm)
- Spacers (6mm - Aluminum)
- Connectors (6mm)

List of Tests

- Solar absorptance
- Heat loss from heater
- PCB - k, C_P, ϵ_{IR}
- Solar Panel - k, C_P, ϵ_{IR}
- Solar cell - ϵ_{IR}

List of Equipment

- Vacuum chamber
- Flexible Heater by DigiKey (KHLVA-0502/5-P)
- Power Supply
- Data Acquisition Computer
- Thermocouples
- NI 9211 thermocouple input module
- High temperature IR paint from Lab IR Paints
- Enclosure for thermal balance tests
- Kapton tape
- Adafruit FT232H - connection between PCB stack and computer to read sensor data
- Torque wrench (Facom A.300A)
- USB-C cable
- JST SH4 cable

Section 3.1 presents the measurement of solar absorptivity for solar cells and panels. Heat loss along the heater power supply wire is examined in Section 3.2. The thermo-optical properties of the PCB and solar panel are determined in Sections 3.3 and 3.4, respectively. Finally, Section 3.5 focuses on the infrared emissivity of the solar cell.

3.1. Solar absorptance test

The exterior of a CubeSat consists of solar panels and solar cells which are exposed to solar heat flux, albedo and earth infrared radiation. Thus, the value of solar absorptivity needs to be determined. This will help predict the thermal behavior of the satellite. This section highlights the measurement procedure, data analysis procedure and results obtained.
Of the methods for measuring solar absorptivity discussed in section 1.1.5, only the UV-Visible spectrometer with an integrating sphere (figure 3.1) was available at TU Delft (Faculty of Applied Sciences). The wavelength band of the machine is from 200 nm to 2500 nm, which covers 96.71% of the solar spectrum[35]. The instrument accepts samples between 20 mm × 20 mm and 35 mm × 35 mm, with a maximum thickness of 8 mm

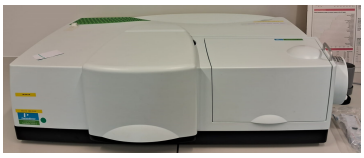

(a) UV-Vis Spectrometer: Perkin Elmer Lambda 1050S

(b) Placement inside integrating sphere

Figure 3.1: Experimental setup for solar absorptivity measurements

3.1.1. Calculation of α_s from raw data

The machine gives raw data of absorbance vs. wavelength which has to be converted into the effective solar absorptance of the sample. The procedure for the same had to be determined and is shown below.

$$A(\lambda) = -\log_{10}\left(\frac{I}{I_0}\right) \tag{3.1}$$

The ratio $\frac{I}{I_0}$ represents the reflection ratio, denoted by r.

$$A(\lambda) = -\log_{10}(r(\lambda)) \tag{3.2}$$
$$r(\lambda) = 10^{-A(\lambda)} \tag{3.3}$$
$$\alpha(\lambda) = 1 - r(\lambda) \tag{3.4}$$
$$\alpha(\lambda) = 1 - 10^{-A(\lambda)} \tag{3.5}$$

The effective solar absorptivity is then calculated as

$$\alpha_s = \frac{\sum \alpha(\lambda)\, E_\lambda}{\sum E_\lambda} \tag{3.6}$$

where,

$A(\lambda)$: absorbance (raw data)

I : intensity measured by sensor

I_0 : incident intensity

$r(\lambda)$: fraction of light reflected

$\alpha(\lambda)$: fraction of light absorbed

E_λ : solar spectral irradiance

α_s : effective solar absorptivity

E_λ corresponds to the solar irradiance which is obtained from the work by Gueymard [35] as shown in figure 3.2. This dataset represents solar irradiance as a function of wavelength, corresponding to a solar constant of 1361 W/m^2. This value is based on updated measurements from 2018, replacing the previously accepted value of 1367 W/m^2.

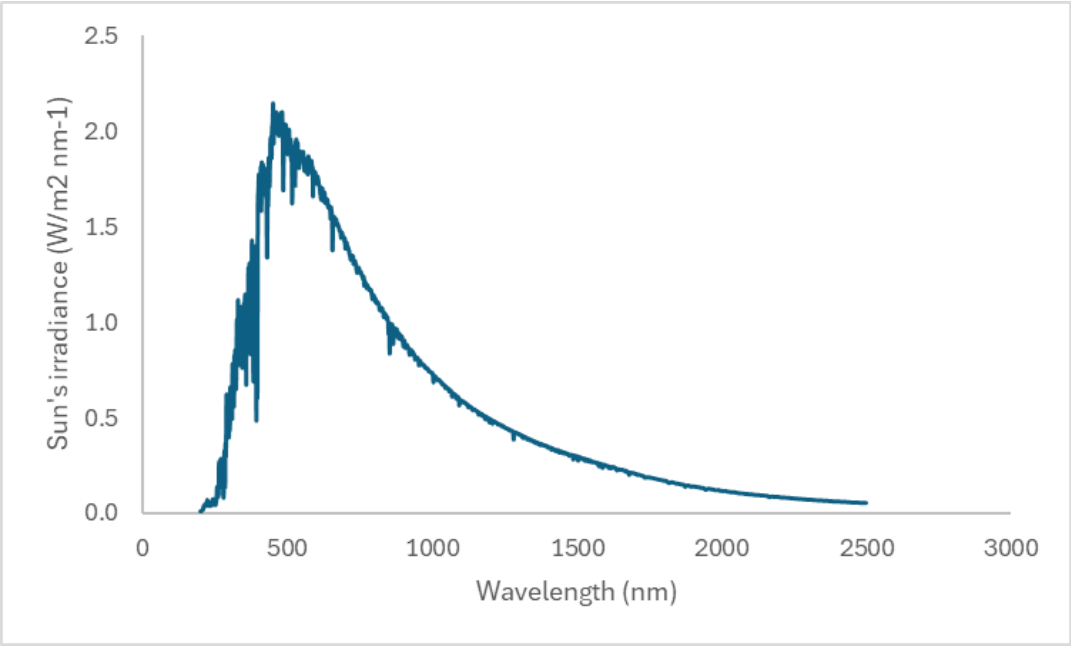

Figure 3.2: Solar Irradiance
[35]

3.1.2. Results

For this test, samples of solar cells and solar panels were cut to a size of 25mm x 25mm, and are shown in figure 3.3.

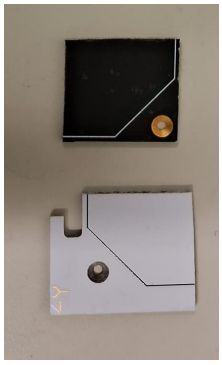

(a) Solar panel samples

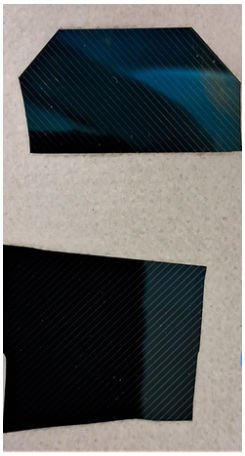

(b) Solar cell samples (A & B)

Figure 3.3: Cut solar panel and solar cell samples

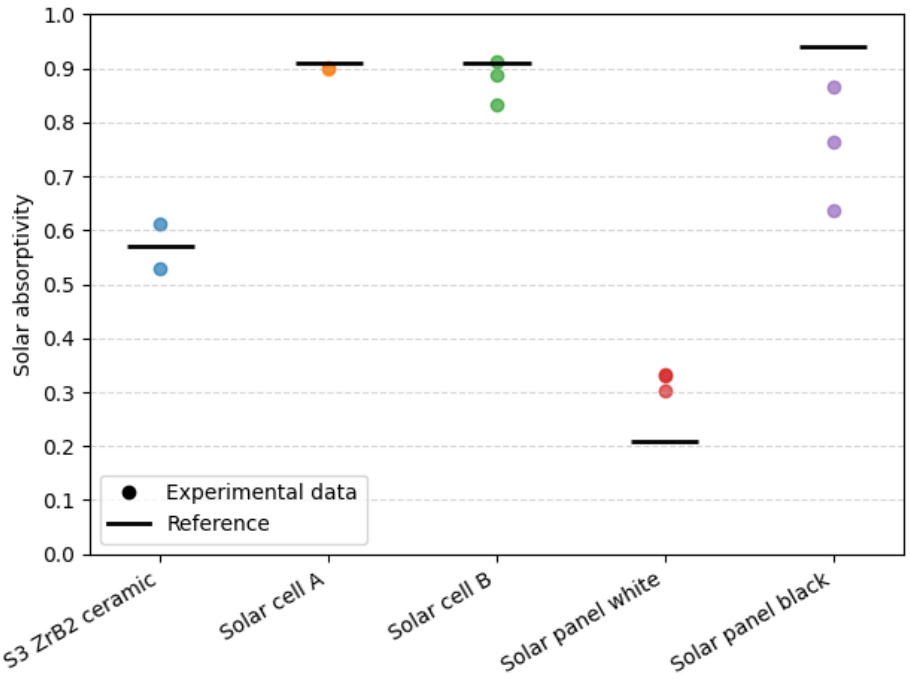

Figure 3.4: Solar absorptivity results with reference values

A sample calculation for the determination of α_s from the raw data has been shown in appendix A.

Table 3.1: Comparison of measured and reference solar absorptivity values

Component	Test 1	Test 2	Test 3	Reference
Ceramic sample	0.53	0.61	–	0.57[36]
Solar Cell (sample A)	0.90	0.89	–	$<$0.91[15]
Solar Cell (sample B)	0.83	0.91	0.89	
Solar Panel (black coating)	0.87	0.64	0.77	0.94[13]
Solar Panel (white coating)	0.30	0.33	0.33	0.21[13]

3.1.3. Discussions

The ceramic sample in the reference has a mean absorptivity value of 0.57. This sample has been chosen as measurements have been made on this sample earlier and can be used to validate the current solar absorptivity determination procedure. The values obtained from the experiments are 0.53 and 0.61 which fall within an error of 4%. Thus, the mathematical manipulation method described in section 3.1.1 can be considered accurate.

Solar cells have an absorptivity ranging from 0.83 to 0.91 which agrees with the value mentioned in the reference. It should be noted that the tested solar cells did not include the cover-glass coating present in the flight configuration.

The values of solar absorptivity of the black solar panel show a very large variation which could be due to the fact that the sample was held too close inside the clipper which led to a small surface area for the beam which itself has a size of 12 mm x 9 mm. It may have been possible that some part of the incident light did not hit the sample at all.

The white solar panel has a value about 50% higher than the reference value. This highlights the fact that coatings can vary significantly and change from supplier to supplier, thus one cannot be sure what a white coating refers to because they have a wide range of optical properties. Also, the work by Kauder [27] highlights that different types of white coatings can lead to solar absorptivities varying from 0.03 to 0.54.

3.2. Heat Loss from heater

This section presents a preliminary test conducted to better characterize the heat flow from the heater used in the thermal balance experiments described in the following sections.

As the primary heat source, the heater reaches the highest temperature during testing. As a result, a portion of the supplied heat is conducted along the power supply wires instead of passing through the test specimen. It is important to account for this effect, as a significant amount of heat is being lost through the wiring.

A polyimide film flexible heater by DigiKey (KHLVA-0502/5-P) is being used.

- power density of $5 W/\text{in}^2$
- 2 inch x 0.5 inch (50.88 mm x 12.7 mm)
- operating temperature up to 150°C

3.2.1. Test description

The heater was attached to a piece of solar panel having the same dimensions as the heater. This setup was covered with LabIR paint[37] to ensure the surface has known emissivity of 0.8. Two thermocouples (TC) were placed on the heater and the wire at locations shown in figure 3.5 using yellow kapton tape. The setup was then hung mid-air using a dyneema thread tied between the power supply wire and the ceiling of the vacuum chamber to avoid any conduction losses from the surface to the walls. The test was conducted at a pressure of 0.12 mbar which is the lowest achieveable pressure in the vacuum chamber available.

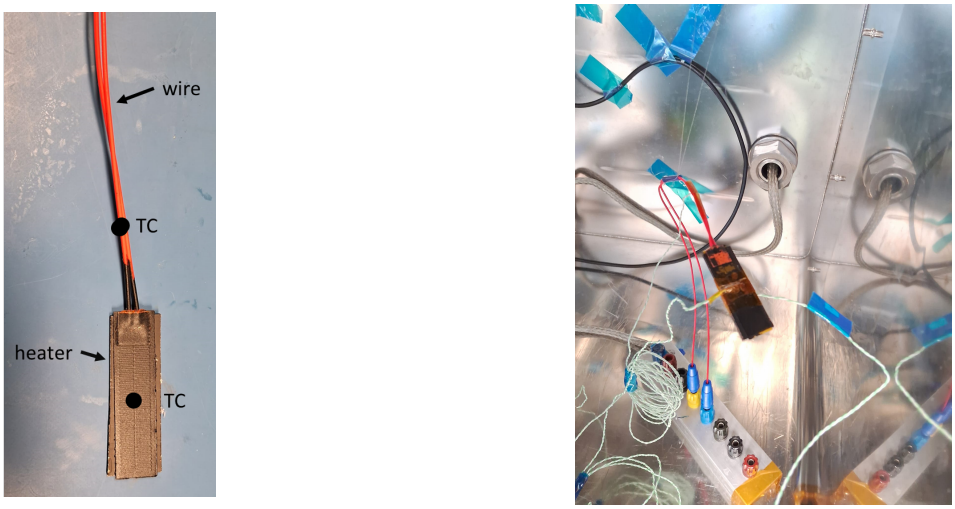

(a) placement of thermocouples

(b) setup inside vacuum chamber

Figure 3.5: Heat loss test setup

Next, a thermal network has been shown that considers a single node with heat input from the tape heater, and heat loss via conduction through the power supply wire and radiation to the walls.

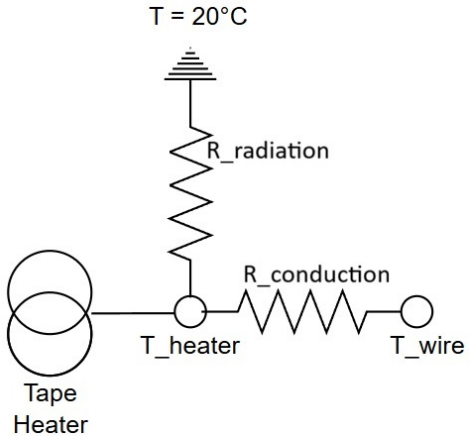

Figure 3.6: Thermal network for heat loss estimation

$$Q_{\text{gen}} = \varepsilon_{\text{heater}} \sigma A_{\text{heater}} T_{\text{heater}}^4 + G L_{\text{heat loss}} \left(T_{\text{heater}} - T_{\text{wire}}\right) \tag{3.7}$$

When steady state is achieved, the heat generated at the heater has three paths:

- radiation from the surface
- convection from the surface
- conduction along power supply wire

Now, the radiation from the surface can easily be calculated as the temperature and emissivity of the surface is known. The remaining heat (conduction along wire + convection from surface) is considered as heat loss from the heater.

3.2.2. Results

The table given below indicates the power supplied to the heater and the corresponding heat loss. Further, an equivalent $\frac{kA}{L}$ is calculated which can act as an **effective heat loss coefficient** for heat loss in future tests.

The test procedure and sample calculation has been shown in Appendix B.2

Table 3.2: Heat loss resistance

Input Power	Heater Temp	Wire Temp	Radiation Loss	Heat Loss	$\mathbf{kA/L}$
0.5W	$44.5\,^{\circ}\mathrm{C}$	$30\,^{\circ}\mathrm{C}$	0.24W	0.26W	$0.018 \pm 0.003\ \frac{\mathrm{W}}{\mathrm{K}}$
1.5W	$92\,^{\circ}\mathrm{C}$	$40\,^{\circ}\mathrm{C}$	0.91W	0.59W	$0.011 \pm 0.002\ \frac{\mathrm{W}}{\mathrm{K}}$

In the measurement of heat loss there are various sources of errors stemming from measurements of power supply, length, surface emissivity and thermocouple accuracy. All of this has been accounted for and we get an effective heat loss coefficient of **0.015** $\pm$ **0.006** $\mathrm{W\,K^{-1}}$.
This value will be used in the thermal balance tests that are performed for the PCB and solar panel.

3.2.3. Convection calculation

Although convection losses have been accounted for in the effective heat loss coefficient, it would be helpful to get an idea of order of magnitude.

The sample is considered to be a temperature of 50°C and the surrounding air is at 20°C. The vacuum chamber pressure is 0.12 mbar. The thermophysical properties for convection calculations were obtained from NIST data using miniREFPROP software.

$$Pr = 0.7053$$

$$k = 0.026945 \text{ W/mK}$$

$$\nu = 1.393 \times 10^{-1} \text{ m}^2/\text{s}$$

$$Ra_D = \frac{g\beta(T_s - T_\infty)D^3}{\nu^2} Pr$$

$$Nu = \left\{ 0.6 + \frac{0.387 Ra_D^{1/6}}{\left[1 + (0.559/Pr)^{9/16}\right]^{8/27}} \right\}^2$$

$$h = \frac{k}{D} Nu$$

This gives a value of h = **0.49 W/**m^2**K**.
For the given sample, this corresponds to a convection heat loss of **0.023 W**.
Note that the actual PCB has an area which is around 3 times that of this sample, which indicates convection loss of 0.069 W if the entire PCB was at the assumed temperature of 50° C.
The heat loss coefficient gives a value of 0.26 W at this temperature which already accounts for convection. Therefore, it can be inferred that the majority of the heat loss occurs due to conduction along the power supply wires. Any additional convection resulting from the larger surface area of the actual PCB remains within the uncertainty bounds of the overall heat loss estimation.

3.3. Printed Circuit Board - k, C_P, ϵ_{IR}

A CubeSat consists of various components like the payload, structure, solar panel, solar cells and various PCBs like the on-board computer, attitude determination and control system, electrical power system. Since a significant portion of a CubeSat consists of PCBs it is important to characterize them. In order to do so, thermal balance tests have been performed for the determination of thermal conductivity, heat capacity and infrared emissivity.

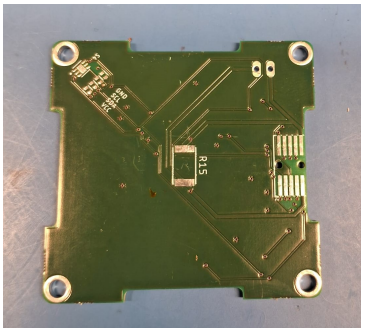

Figure 3.7: PCB

3.3.1. Test setup

A tape heater is attached to one edge of the PCB, with thermocouples positioned at distances of 24 mm and 37 mm from that edge along which the heater is placed as shown in figure 3.8

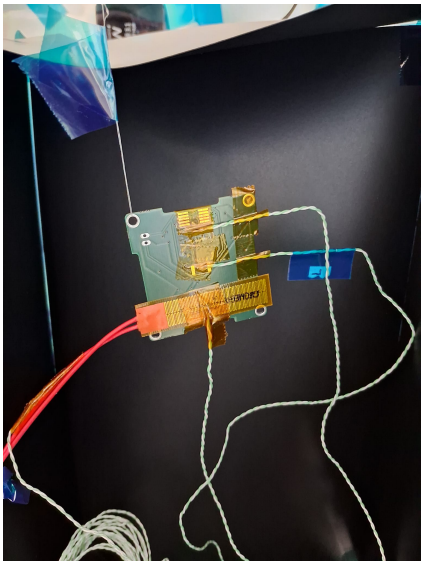

(a) PCB inside enclosure with heater and thermocouples attached

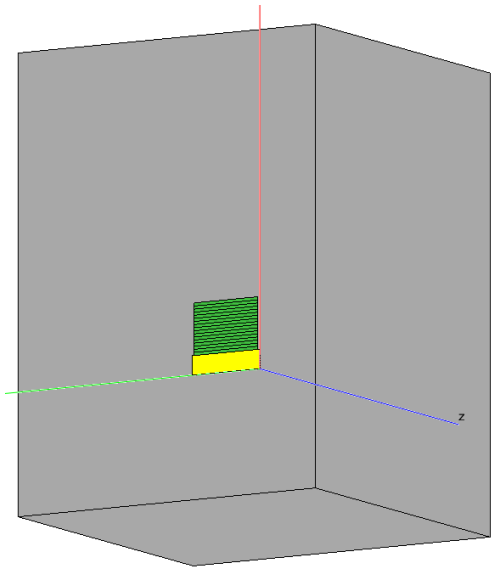

(b) ESATAN Model

Figure 3.8: Comparison of experimental setup and ESATAN model

The test is carried out inside the vacuum chamber at a pressure of 0.12 mbar.

An important aspect for these tests is the radiation exchange with the walls of the chamber. Since the emissivity of the walls is unknown, a six-sided enclosure made from A4 sheets was constructed whose inner surface was coated with the LabIR paint (Figure 3.9). Now, the radiative exchange factor can be easily determined using ESATAN and be used during the steady state calculations.

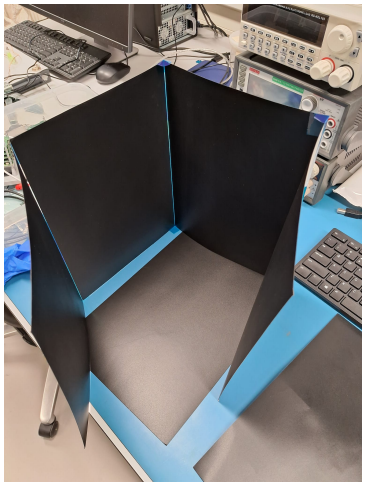

Figure 3.9: Enclosure with inner surface of known emissivity

The detailed test procedure is shown in appendix C.1.

For representation purposes, the thermal network considers the PCB to be divided into 4 elements.

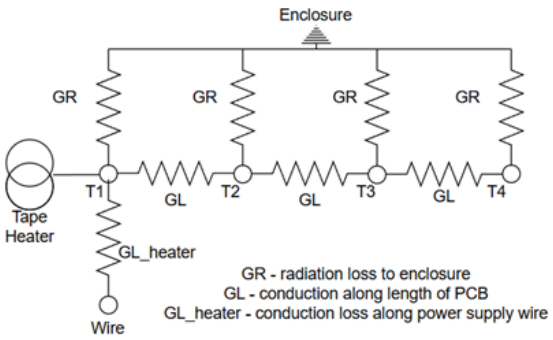

Figure 3.10: Thermal network for PCB

Heat supplied to the PCB during steady state will flow through three paths:

- radiation from the surface (GR)
- conduction along the length of the surface, away from the heater (GL)
- heat loss using the effective heat loss resistance described in section (GL _ heater)

For the purposes of calculation of thermal properties, the PCB was divided into 18 elements based on a convergence study performed in ESATAN.

The steady state heat balance equations have been described below:

Equation 3.8 refers to the steady state equation for the first element that represents the element with the heater.

Equation 3.9 refers to the middle elements that receive heat by conduction and lose heat via radiation and conduction.

Equation 3.10 refers to the last element that receives heat by conduction and loses heat via radiation alone.

$$Q_{\text{gen}} + \frac{kA_{\text{cond},1}}{L_1}(T_2 - T_1) - \varepsilon\sigma A_{\text{rad},1}B(T_1^4 - T_\infty^4) = 0 \tag{3.8}$$

$$\frac{kA_{\text{cond},i-1}}{L_{i-1}}(T_{i-1} - T_i) + \frac{kA_{\text{cond},i}}{L_i}(T_{i+1} - T_i) - \varepsilon\sigma A_{\text{rad},i}B(T_i^4 - T_\infty^4) = 0 \tag{3.9}$$

$$\frac{kA_{\text{cond},N-1}}{L_{N-1}}(T_{N-1} - T_N) - \varepsilon\sigma A_{\text{rad},N}B(T_N^4 - T_\infty^4) = 0 \tag{3.10}$$

where,

Q_{gen} : Heat generation/input at the first node [W]
k : Thermal conductivity of the material [W/m·K]
$A_{\text{cond},i}$: Cross-sectional area for conduction between nodes i and $i+1$ [m^2]
L_i : Distance between nodes i and $i+1$ [m]
T_i : Temperature at node i [K]
ε : Surface emissivity [-]
σ : Stefan–Boltzmann constant (5.67×10^{-8} W/m^{2}K^4)
$A_{\text{rad},i}$: Radiating surface area at node i [m^2]
T_∞ : Ambient temperature [K]
B : Radiative exchange factor from PCB to walls of enclosure = 0.988 (calculated from ESATAN model)

For the thermal network under consideration, two parameters remain unknown in the steady-state heat balance: the thermal conductivity, k, and the infrared emissivity, ϵ_{IR}.
To solve this issue 2 experiments have been designed and performed as explained in the flowchart below.

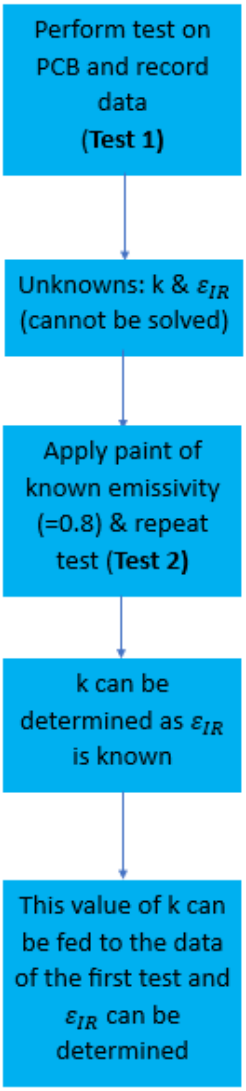

Figure 3.11: Testing sequence for PCB

3.3.2. Results

For **Test 1**, without the paint, a power of 0.5W was supplied and the resulting temperatures achieved during steady state are shown in figure 3.12. This data is stored using a labview script that logs the data of temperature vs time in an excel file.

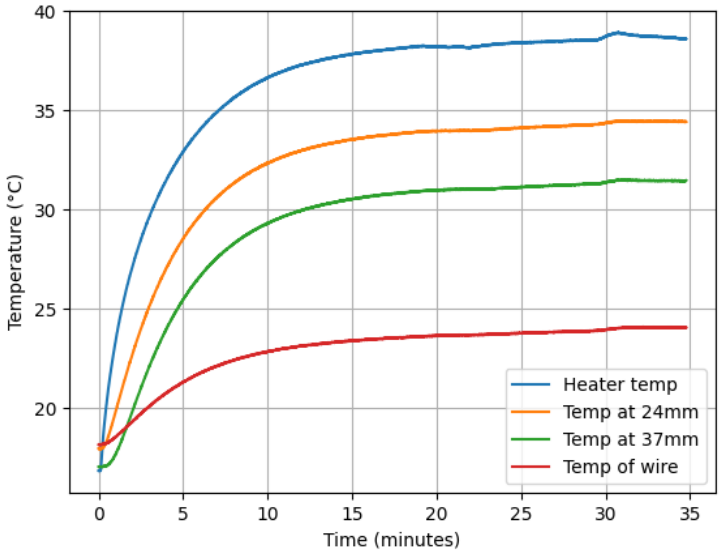

Figure 3.12: Temperature of PCB as a function of time for **Test 1**

Now, we move to **test 2** as per the flowchart which involves repeating the test after applying paint to the sample.

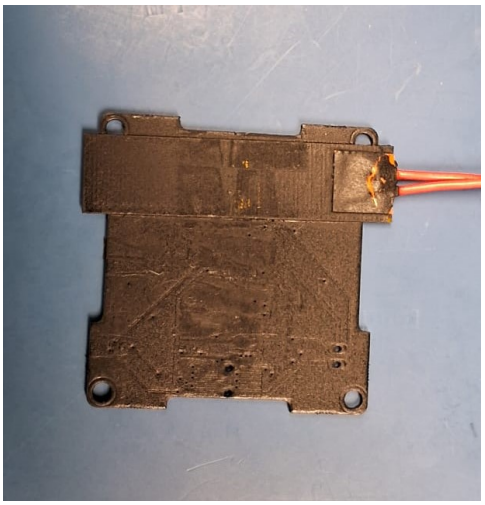

Figure 3.13: PCB and heater after paint application

The steady state temperatures from this test are shown in figure 3.14.

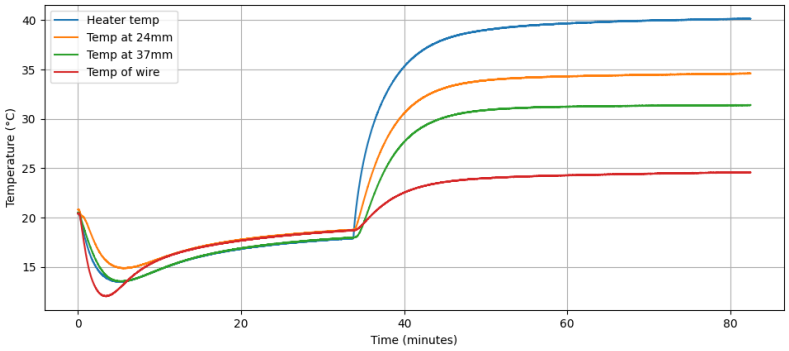

Figure 3.14: Temperature of PCB as a function of time for **Test 2**

One thing to note is that we can make a prediction about the emissivity value of the PCB by just looking at the temperatures of the steady state of both tests. The temperatures of the PCB, for the same power input, are lower without the paint. This implies that the emissivity of the PCB is higher than that of the paint (ϵ_{IR} = 0.8).

Now, the data of Test 2 will be analyzed first to obtain the thermal conductivity and then used in data of test 1 to determine the infrared emissivity of the PCB.

A code has been written to solve the steady state equations described earlier. The errors in the measurements have been accounted for and this results in a range of values for thermal conductivity and infrared emissivity.

- Thermocouple accuracy: $\pm$2.2 K
- Power supply error: 0.064 W
- Paint emissivity error: $\pm$0.013 (given by supplier)

Table 3.3: Code Inputs

Parameter	**Value**	
PCB dimensions	$47 \times 47 \times 1.59$ mm^3	
Paint emissivity	0.8 ± 0.013	
Input power	0.5 W	
Heat loss	0.14 to 0.32 W	
Temperature readings	**Test 1**	**Test 2**
TC 1	38.5	40.1°C
TC 2	34.2	34.6°C
TC 3	31.2	31.4°C
TC accuracy	± 2.2 K	
Ambient temperature	20°C	

Finally, for the determination of heat capacity, the power was turned up to a value of 1.5 W and then the heater was turned off at the end of test 2 and the transient data of temperature vs time was logged. A code has been written that considers the steady state temperatures as input and models heat loss by radiation and conduction from the elements. The results of the same are shown in figure 3.15

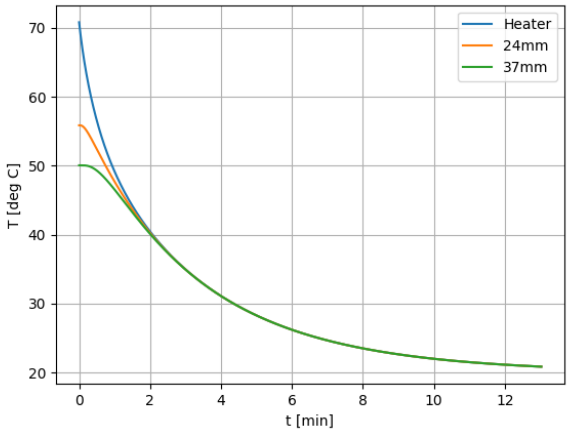

(a) Transient phase modeling (code)

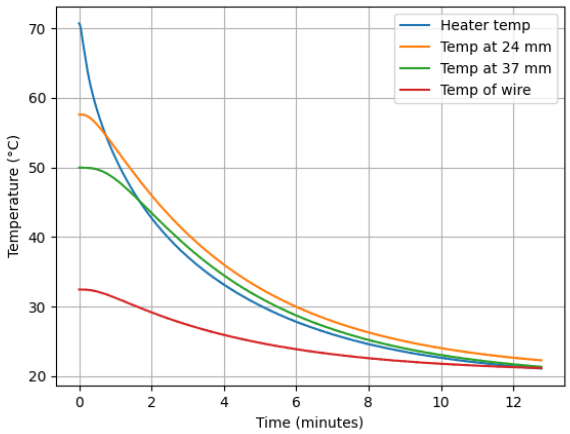

(b) Transient phase (experiment)

Figure 3.15: Comparison of transient thermal response for PCB

Table 3.4: Code Outputs

Parameter	**Value**
Thermal conductivity	10 ± 5 W/mK
Infrared emissivity	0.86 ± 0.06
Heat capacity	550 ± 40 J/kg·K

3.3.3. ESATAN validation of code

The test 1 setup has been replicated in ESATAN and the properties obtained from the code will be used to model the PCB to check whether the temperature distribution is the similar to that obtained from the thermocouple readings of the experiment.

Geometry

The PCB was modeled as a shell of size 47 mm X 47 mm, having a thickness of 1.59mm. The PCB was divided into 18 faces. Further, the enclosure placed around the PCB was modelled as a box with emissivity of 0.8.

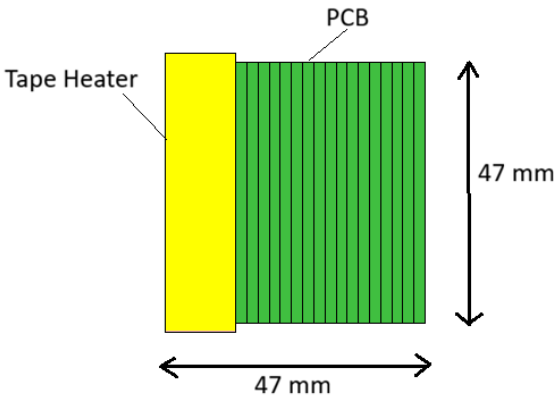

Figure 3.16: PCB model - discretized

Material Properties

The material properties listed in table 3.4 have been used.
k = 10 W/mK
ϵ_{IR} = 0.86
C_P = 550 J/kgK

Boundary Conditions

The first element (shown in yellow in figure 3.16) was given a Total area heat load considering heat losses along the wire. Based on data given in table 3.6, the heat input was varied from 0.18 W to 0.36 W.

Simulation results

The results obtained from the simulation have been compared with the experimental results as shown in figure 3.17.

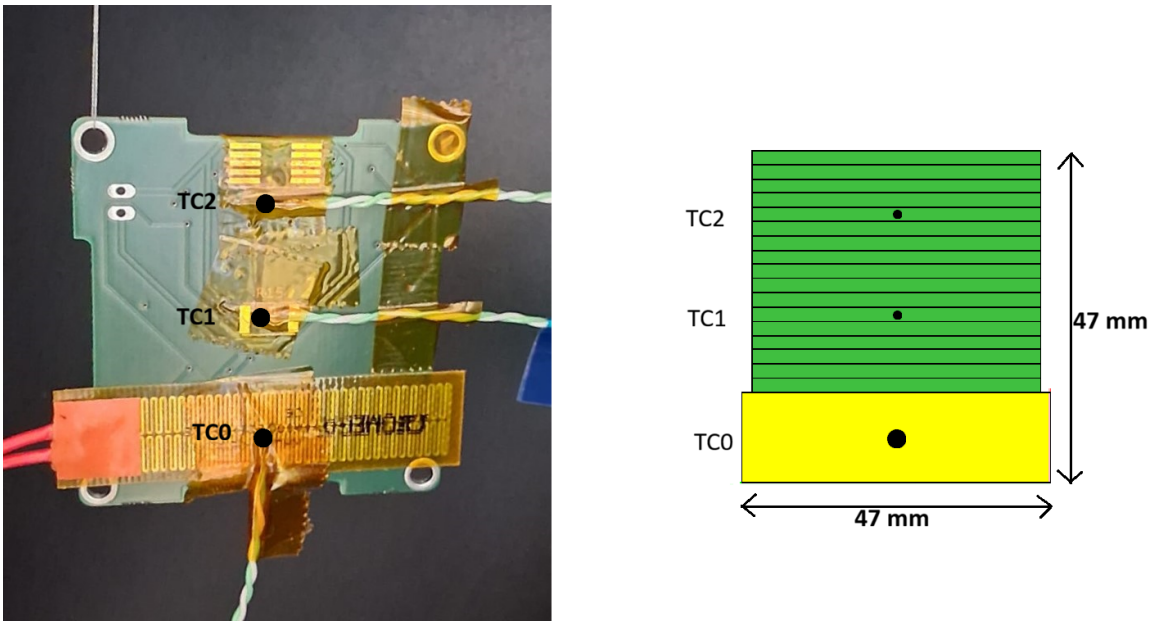

Figure 3.17: Experiment vs ESATAN comparison

Thermocouple Location	Experimental Value	ESATAN Results	|Difference (%)|
TC0	38.5°C	37.0°C	3.9%
TC1	34.2°C	33.5°C	2.0%
TC2	31.2°C	32.1°C	2.9%

Table 3.5: Comparison of experimental and ESATAN temperature results with percentage difference

The temperature at respective nodes are within $\pm$2.2 K which falls within the thermocouple accuracy.

3.4. Solar Panel - k, C_P, ϵ_{IR}

Solar Panels form the outer surface of cubesats and are exposed to heat flux from the sun, albedo and Earth infrared radiation. Thus it is important to understand their thermal behavior which requires determination of the thermal and optical properties.

The panels are very similar to the PCB in their buildup, with the difference being the amount of copper used. The test setup and sequence will be the same as that used for the PCB and thus the results and images of the test have been directly shown without explanation of the test procedure.

An important nomenclature from the previous subsection is that **Test 1** refers to the test without the application of paint, while **Test 2** refers to the test after application of the paint.

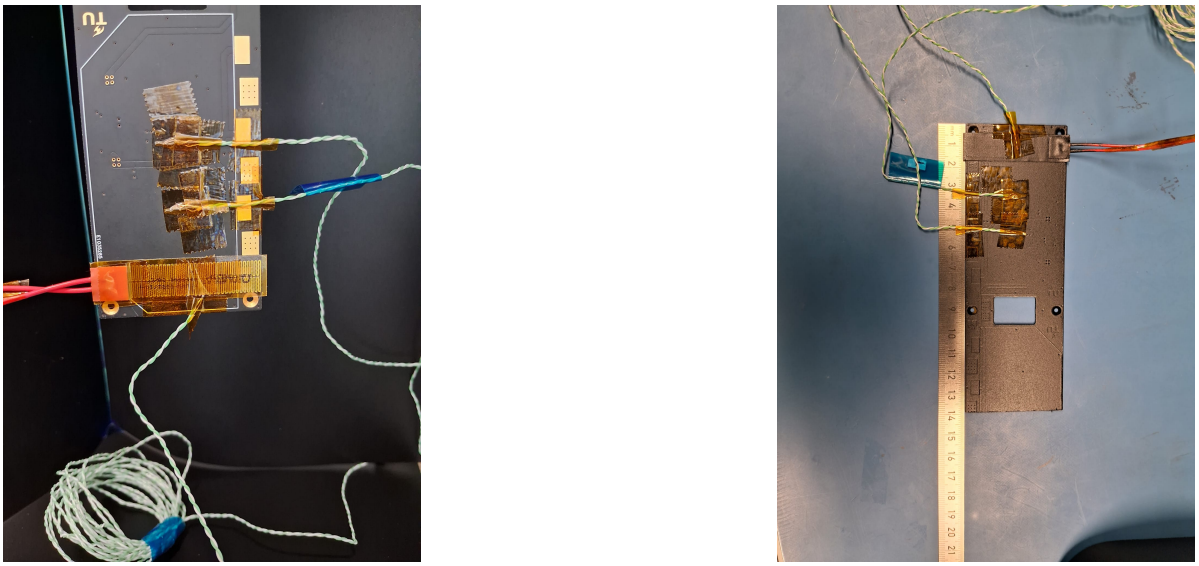

(a) Test 1 - without paint

(b) Application of paint on solar panel

Figure 3.18: Thermal balance tests for the solar panel

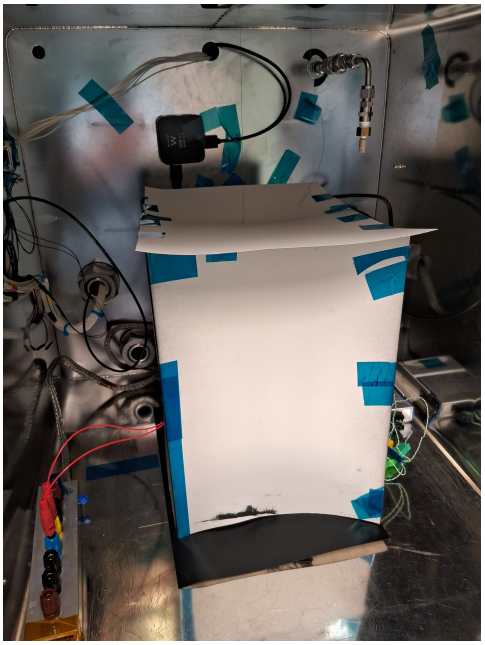

Figure 3.19: Thermal balance test setup of solar panel inside enclosure

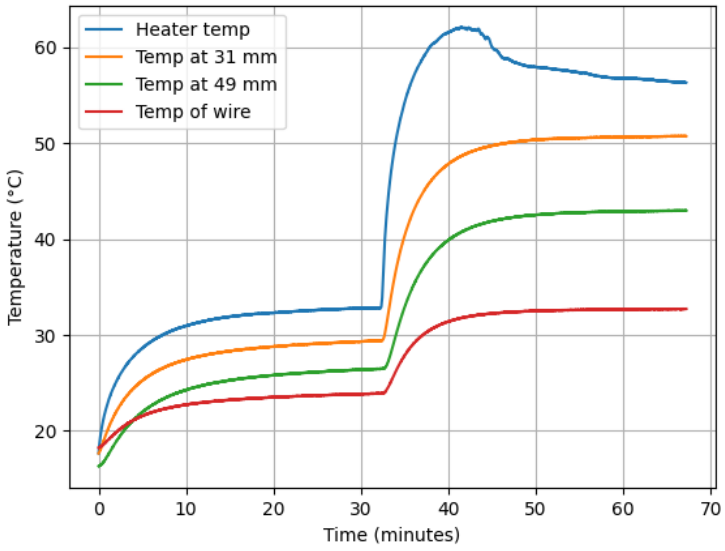

Figure 3.20: Temperature of Solar Panel as a function of time for **Test 1**

In the results for test 1 shown in figure 3.20, the initial steady state achieved corresponds to a power of 0.56 W for which the data has been analyzed. The second steady steady state achieved at higher power was an attempt to generate another set of data points, but the thermocouple got detached from the heater which led to decrease in temperature as seen in the graph.

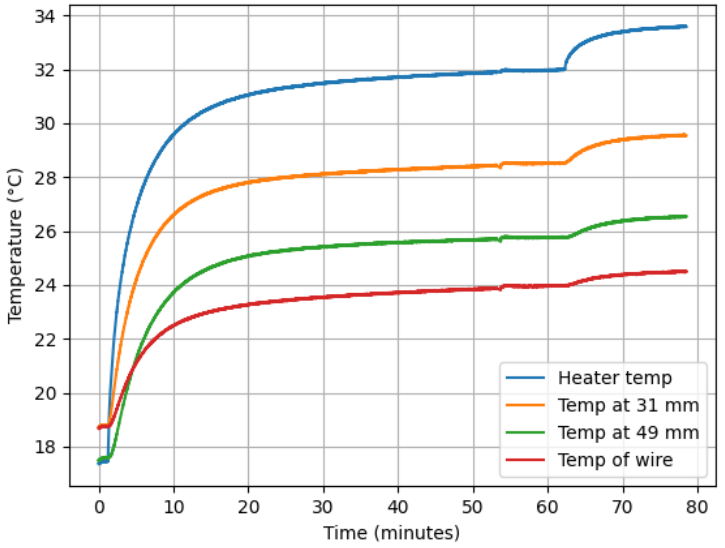

Figure 3.21: Temperature of Solar Panel as a function of time for **Test 2**

The graph in figure 3.21 has a rise in temperature at the end as the initial voltage provided was slightly lower than required. It was subsequently increased to 6.8 V to achieve the target power of 0.566 W.

Table 3.6: Code Inputs

Parameter	**Value**	
Panel dimensions	$140 \times 50 \times 1.59$ mm^3	
Paint emissivity	0.8 ± 0.013	
Input power	0.56 W	
Heat loss	0.08 to 0.19 W	
Temperature readings	**Test 1**	**Test 2**
TC 1	32.8°C	33.6°C
TC 2	29.4°C	29.6°C
TC 3	26.5°C	26.5°C
TC accuracy	± 2.2 K	
Ambient temperature	20°C	

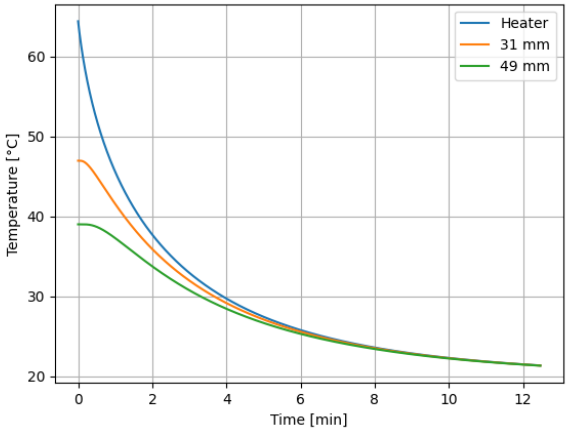

(a) Transient phase modeling (code)

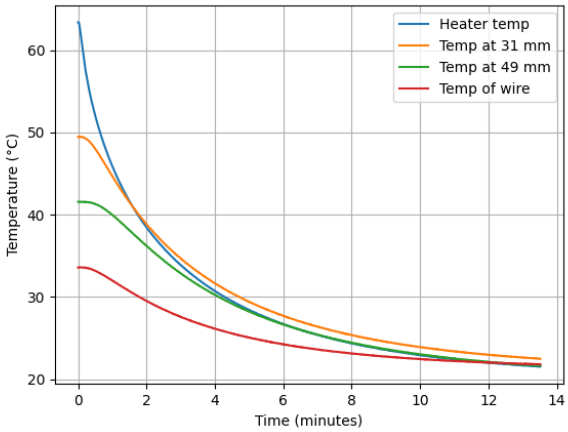

(b) Transient phase (experiment)

Figure 3.22: Comparison of transient thermal response for Panel

Table 3.7: Code Outputs

Parameter	Value
Thermal conductivity	25 ± 15 W/mK
Infrared emissivity	0.9 ± 0.1
Heat capacity	630 ± 130 J/kg·K

3.4.1. ESATAN validation of code

The test 1 setup has been replicated in ESATAN and the properties obtained from the code will be used to model the solar panel to check whether the temperature distribution is the similar to that obtained from the thermocouple readings of the experiment.

Geometry

The panel was modeled as a shell of size 140 mm X 50 mm, having a thickness of 1.59 mm. The panel was divided into 78 faces. Further, the enclosure placed around the panel was modeled as a box with emissivity of 0.8.

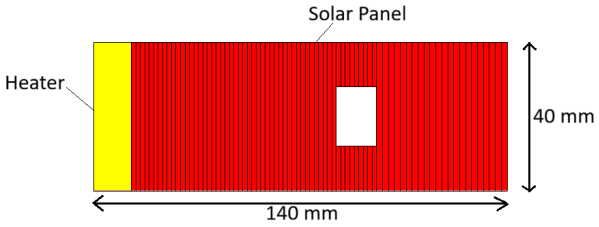

Figure 3.23: Panel model - discretized

Material Properties

The material properties listed in table 3.7 have been used.
k = 25 W/mK
ϵ_{IR} = 0.9
C_P = 630 J/kgK

Boundary Conditions

The first element (shown in yellow in figure 3.16) was given a Total area heat load considering heat losses along the wire. Based on data given in table 3.6, the heat input was varied from 0.37 W to 0.48 W.

Simulation results

The results obtained from the simulation have been compared with the experimental results as shown in figure 3.24.

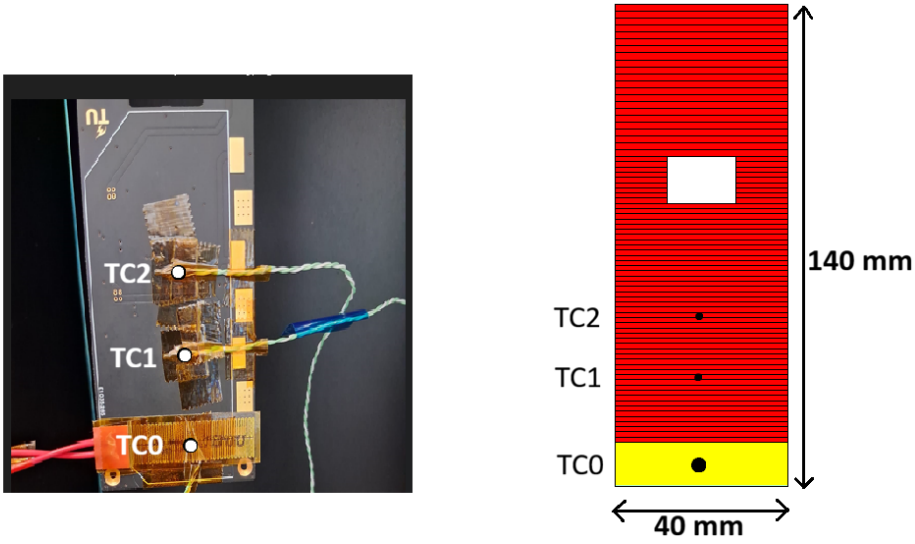

Figure 3.24: Experiment vs ESATAN comparison

Thermocouple Location	Experimental Value	ESATAN Results	|Difference %|
TC0	26.5°C	27.8°C	4.91%
TC1	29.4°C	29.2°C	0.68%
TC2	32.8°C	32.3°C	1.52%

The temperature at respective nodes are within $\pm$2.2 K which falls within the thermocouple accuracy.

3.5. Solar Cell - ϵ_{IR}

Solar cells cover a major area of the surface of solar panels - around 70% in the case of Delfi-PQ. They radiate heat back into space ,thus it is important to account for their infrared emissivity. This value will also be equal to the absorptivity for the infrared radiation from Earth.

Initially, it was decided to create a thermal balance test setup which would involve putting a thermocouple on the heater and/or solar cell to measure the temperature. The heater would be painted using the LabIR Paint to ensure a known emissivity of 0.8. Next, a thermal network has been shown that considers a single node with heat input from the tape heater, and heat loss via conduction through the power supply wire and radiation to the walls.

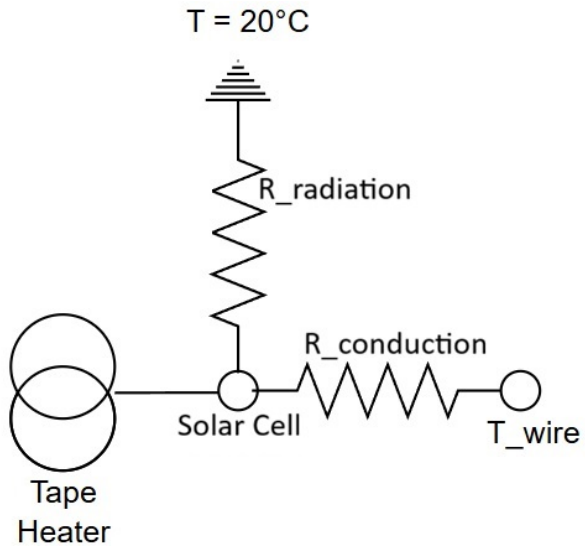

Figure 3.25: Thermal network for solar cell

The steady state equation for the thermal network can be represented by:

$$Q_{\text{gen}} = \varepsilon_{\text{heater}} \sigma A_{\text{heater}} T_{\text{heater}}^4 + \varepsilon_{\text{solar cell}} \sigma A_{\text{solar cell}} T_{\text{solar cell}}^4 + GL_{\text{heat loss}} \left(T_{\text{heater}} - T_{\text{wire}}\right) \tag{3.11}$$

where: Q_{gen} is the generated heat [W],
$\varepsilon_{\text{heater}}$ is the emissivity of the heater [-],
$\varepsilon_{\text{solar cell}}$ is the emissivity of the solar cell [-],
σ is the Stefan–Boltzmann constant [5.67×10^{-8} W/m^{2}K^4],
A_{heater} is the heater area [m^2],
$A_{\text{solar cell}}$ is the solar cell area [m^2],
T_{heater} is the heater temperature [K],
$T_{\text{solar cell}}$ is the solar cell temperature [K],
$GL_{\text{heat loss}}$ is the conductance loss to the wire [W/K],
T_{wire} is the wire temperature [K].

The only unknown in the above equation is the emissivity of the solar cell. The steady state temperatures obtained from the thermal balance test have been shown in figure 3.27.

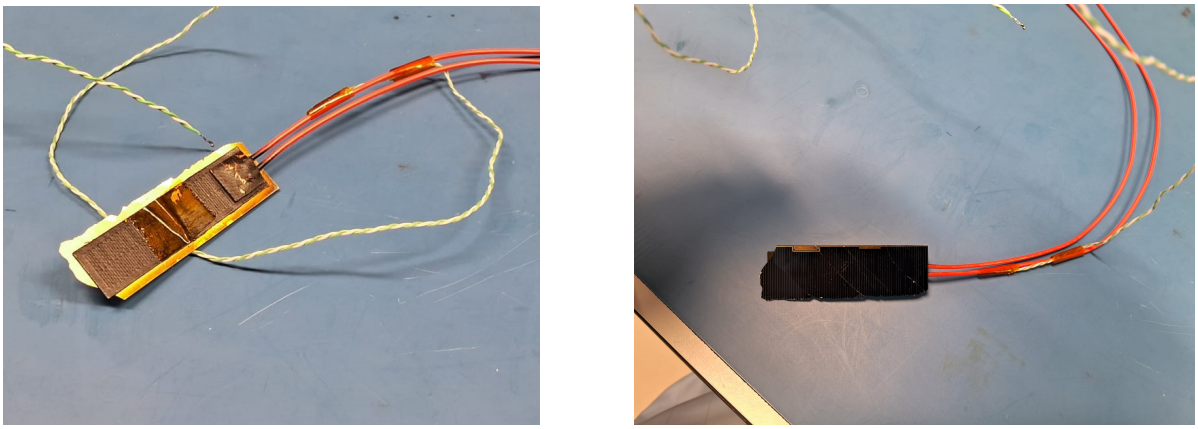

Figure 3.26: Thermal Balance Test for Solar Cell

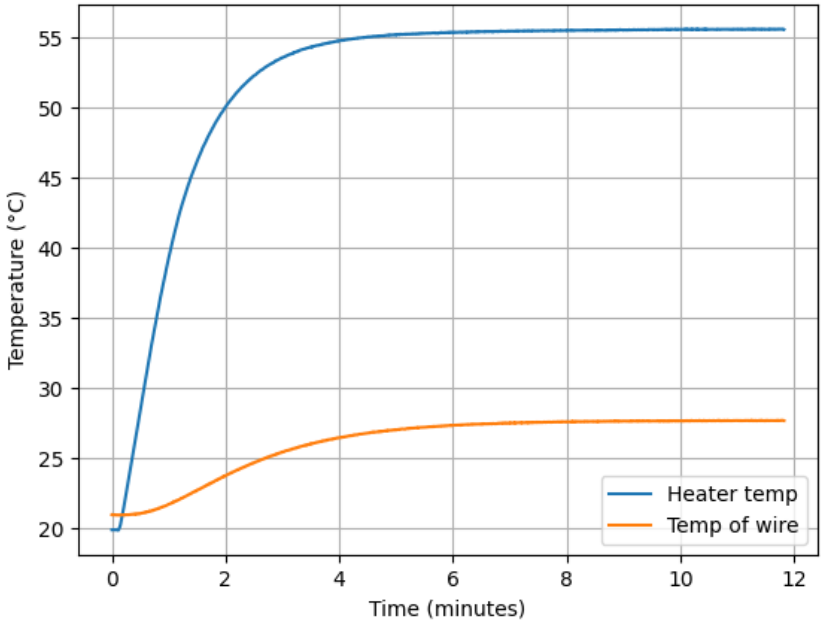

Figure 3.27: Steady state results of thermal balance test

Based on the steady state temperatures from the thermal balance test, the emissivity of the solar cell has been obtained using equation 3.11. This gives a value of **0.88**$\pm$**0.12**.

The value obtained has a very high uncertainty because of the thermocouple accuracy. Thus, these results are not very useful.

In order to get a more accurate value of emissivity, a thermal camera was used. For this test, a small piece of the solar cell was attached to the heater as shown in figure 3.28.

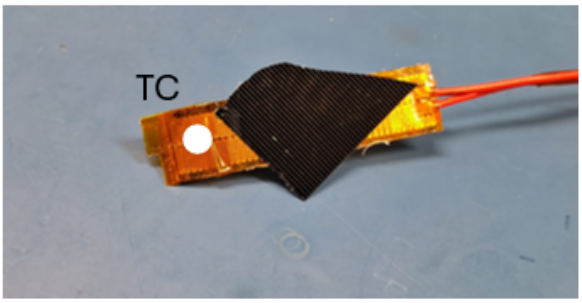

Figure 3.28: IR camera test setup

By changing the power given to the sample via the heater two different temperature states were considered. At both power levels, the temperature is measured both via the infrared camera as well as the thermocouple. The only constant is the surrounding radiation reflected by the solar cell. With these data the infrared emissivity of the sample can be calculated assuming it is constant at both temperatures.

The emissivity of the thermal camera is est to unity:

$$\varepsilon_{\text{cam}} = 1 \tag{3.12}$$

The radiation balance measured by the camera can be written as:

$$\sigma A T_{\text{cam}}^4 = \varepsilon_{solarcell} \sigma A T_{\text{solarcell}}^4 + Q_{\text{refl}} \tag{3.13}$$

By changing the heater power, two different temperature states are obtained:

$$\sigma A T_{\text{cam},1}^4 = \varepsilon_{solarcell} \sigma A T_{\text{solarcell},1}^4 + Q_{\text{refl}} \tag{3.14}$$

Here, the reflected surrounding radiation Q_{refl} is assumed to be constant, and the emissivity ε of the solar cell is assumed to be the same at both temperatures.

Thus, these two equations can be solved to determine the emissivity of the solar cell.

This approach also yielded results with high uncertainty, comparable to those from the thermal balance test; the results are therefore considered inconclusive.

The value given by the cover-glass supplier[14] of $>$0.86 will be used for the sensitivity analysis in the future.

3.6. Discussion

The experimental thermo-optical properties have been summarized in table 3.8.

For the PCB, thermal balance tests helped us determine the heat capacity, emissivity and thermal conductivity. The value of heat capacity is important for the PCBs because they have been used as the upper and lower panels for Delfi-PQ. This is in order to account for temperature fluctuations due to sunlit and eclipse side in an orbit. Since, Delfi-PQ is a pocket-cube, it will experience more fluctuations than a CubeSat because of the lower mC_P term in the equation:

$$Q = mC_P\Delta T$$

For the solar panel, in addition to the thermal balance tests a spectrophotometer with an integrating sphere was used to obtain the solar absorptivity. This device was available at the Applied Sciences Faculty of TU Delft without which it would have been difficult to measure the solar absorptivity values. It is to be noted that this is an expensive machine and usually universities would not have access to this easily.

For the solar cell, the emissivity value has been obtained from the datasheet [14] as the experimental results yielded results that were inconclusive because of the uncertainty in the thermocouples (±2.2 K). Therefore, a value provided from its datasheet[14] has been used. It would have been better to rely on the Invenio machine at the Aerospace Faculty, but it is yet to be calibrated and not very straightforward to use.

Component	Property	Value
PCB	Heat Capacity	(550 ± 40) J/kgK
	Emissivity	0.86 ± 0.06 $[-]$
	Thermal Conductivity (k)	(10 ± 5) W/mK
Solar Panel	Heat Capacity	(660 ± 130) J/kgK
	Emissivity	0.9 ± 0.1 $[-]$
	Solar Absorptivity	0.77 ± 0.1 $[-]$
	Thermal Conductivity (k)	(25 ± 15) W/mK
Solar Cell	Emissivity	0.93 ± 0.07 $[-]$
	Solar Absorptivity	0.61 ± 0.03 $[-]$

Table 3.8: Material properties used for sensitivity analysis

The solar cell absorptivity has been measured using the spectrophotometer and added to the table after considering a 30% efficiency for the solar cells.

4

Sensitivity Analysis

The thermal model developed in chapter 2 will be used along with the property values obtained from the experiments outlined in chapter 3 to perform a temperature sensitivity analysis.

As compared to a sensitivity analysis that helps determine the temperature sensitivity of properties to give a general trend, this study will consider a slightly different approach. The experimentally obtained thermo-optical properties will be varied within their uncertainty range and the change in temperature will be used to update the temperature bounds of the components usually given by manufacturers as shown in table 4.1.

This is important because their may be properties that may have very high uncertainties but their sensitivity may be negligible or the other way around.

Table 4.1: Temperature requirements of the components

Component	Minimal temperature [°C]	Maximal temperature [°C]
PCBs	-20	+60
Solar Cells	-100	+100
Battery	0	+45

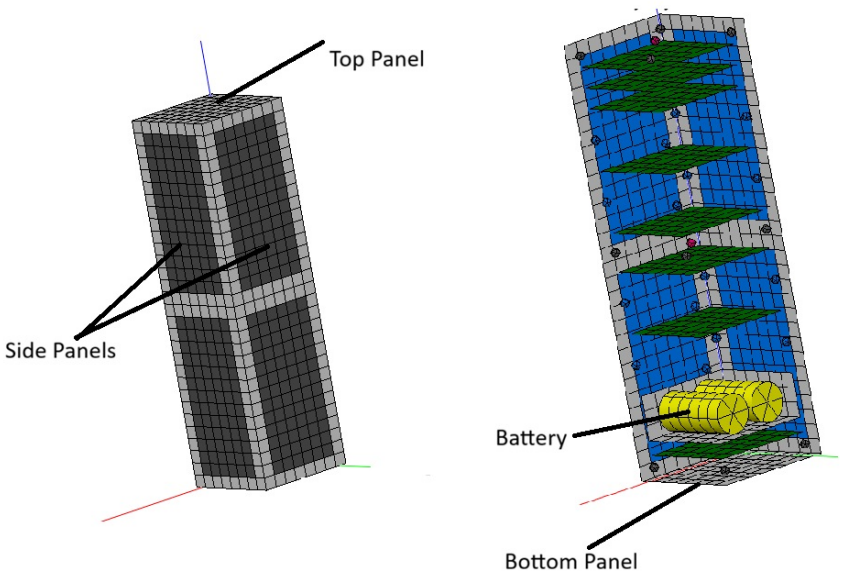

Figure 4.1: ESATAN Model for sensitivity analysis

The table 4.2 contains the values obtained experimentally that will be used for the sensitivity analysis in the following sections of this chapter.

Component	Property	Value
PCB	Heat Capacity ($J\,kg^{-1}\,K^{-1}$)	550 ± 40
	Emissivity (-)	0.86 ± 0.06
Solar Panel	Heat Capacity ($J\,kg^{-1}\,K^{-1}$)	660 ± 130
	Emissivity (-)	0.9 ± 0.1
	Solar Absorptivity (-)	0.77 ± 0.1
Solar Cell	Emissivity (-)	0.93 ± 0.07
	Solar Absorptivity (-)	$0.61 \pm 0.03^*$

Table 4.2: Material properties used for sensitivity analysis

*Considering 30% efficiency of solar cells[15].

4.1. Sensitivity analysis results

4.1.1. Solar Panel emissivity

The solar panel emissivity has been varied from 0.8 to 1.
It can be observed that increasing that solar panel emissivity reduces the overall temperatures which is expected because there is more heat loss, via radiation, to space. From the results of the average battery temperature, it can be seen that a lower solar panel emissivity increases (by $9°C$) the battery temperature, which could be useful when thinking of thermal control solutions.

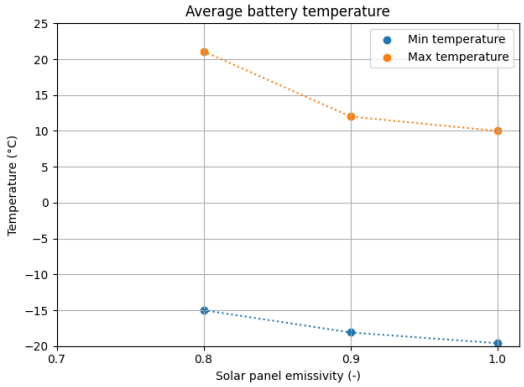

(a) Average Battery Temperature

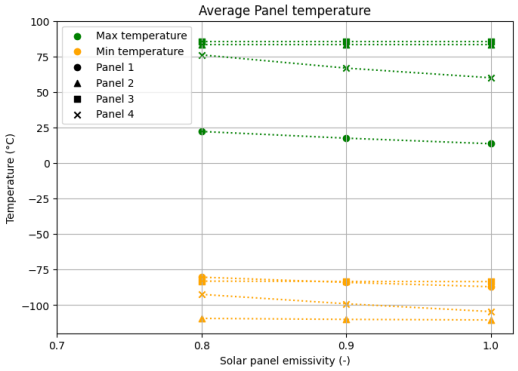

(b) Average temperature of individual solar cells on the 4 side panels

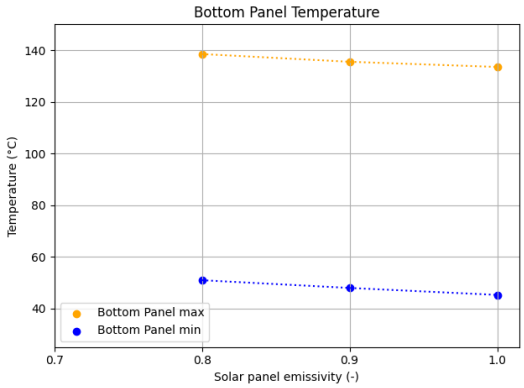

(c) Bottom Panel Average Temperature

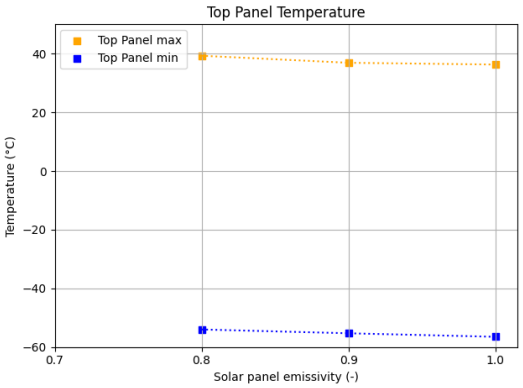

(d) Top Panel Average Temperature

Figure 4.2: Changes in temperatures with varying solar panel emissivity

4.1.2. Solar Panel absorptivity

The solar panel absorptivity is varied from 0.67 to 0.87.
Increasing the solar panel absorptivity leads to more heat absorption by the satellite which translates to higher temperatures.

The effect is seen majorly on the average maximum temperature of the panels because the maximum temperature would be observed when the satellite is on the sunlit side which implies direct heat flux from the sun. The average minimum temperature corresponds to the eclipse side where the solar heat flux is negligible (in the form of albedo) and thus negligible change in its value is seen with change in solar absorptivity.

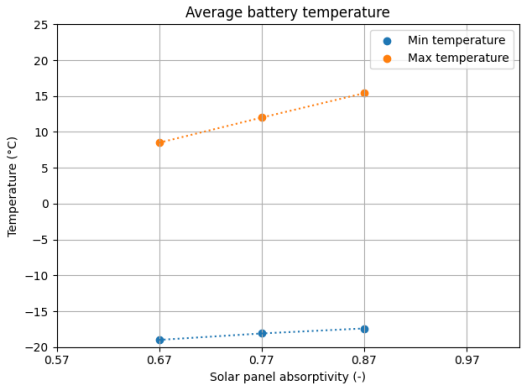

(a) Average Battery Temperature

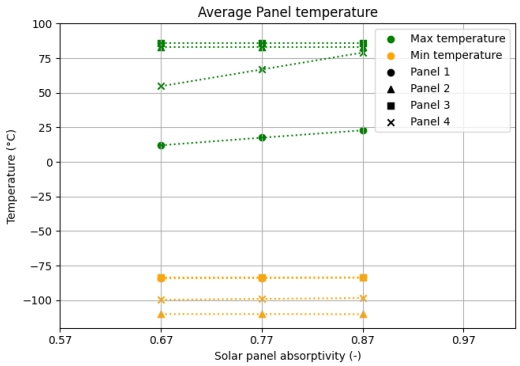

(b) Average temperature of individual solar cells on the 4 side panels

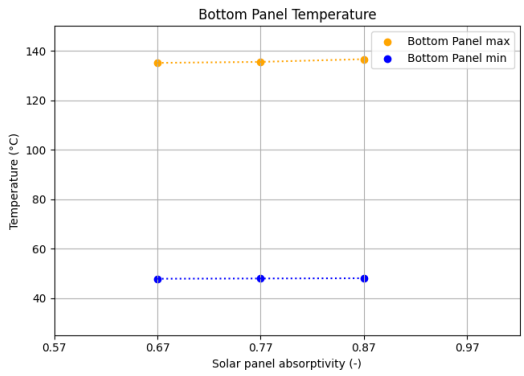

(c) Bottom Panel Average Temperature

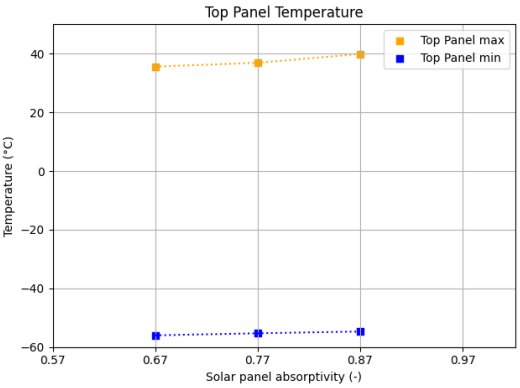

(d) Top Panel Average Temperature

Figure 4.3: Changes in temperatures with varying solar panel absorptivity

4.1.3. Solar panel heat capacity

The solar panel heat capacity is varied from 530 J/kgK to 790 J/kgK.
Increasing the heat capacity implies that the satellite has to spend more time in the given heat flux to attain a given change in temperature. This means that at higher heat capacity values, the satellite will experience a reduction in temperature fluctuations because the time in orbit and heat flux at different locations is constant.

$$Q = mC_p\Delta T \tag{4.1}$$

where, Q is the total heat input
m is the mass of the satellite,
C_p is the heat capacity and
ΔT is the change in temperature

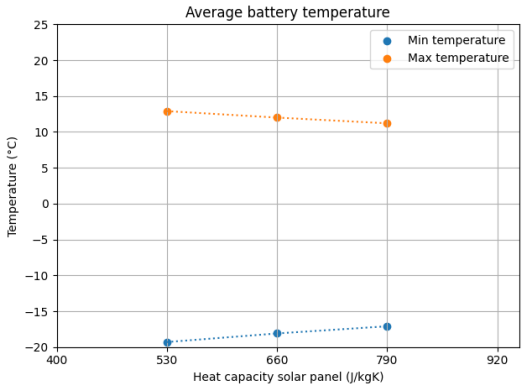

(a) Average Battery Temperature

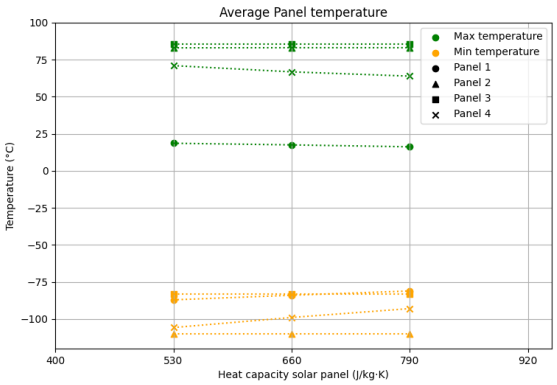

(b) Average temperature of individual solar cells on the 4 side panels

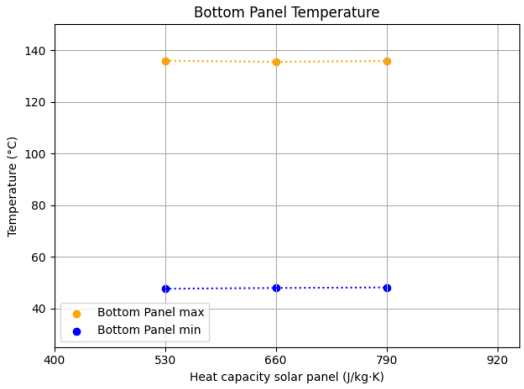

(c) Bottom Panel Average Temperature

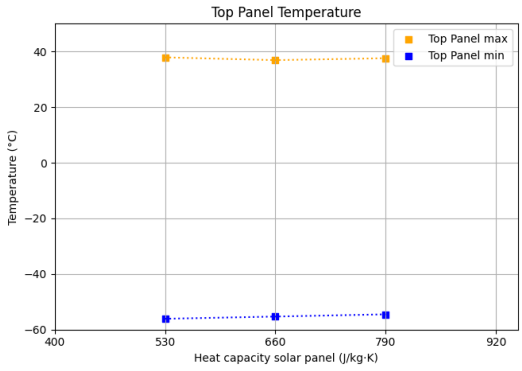

(d) Top Panel Average Temperature

Figure 4.4: Changes in temperatures with varying solar panel heat capacity

4.1.4. Solar cell absorptivity

The solar cell absorptivity is varied from 0.58 to 0.64.
Solar cell absorptivity should have a similar effect as that of increasing solar panel absorptivity which is the increase in temperatures. Although it can be noted that the battery temperature does not vary significantly. This is because the solar cells are glued to the solar panels, which introduces a thermal resistance, and thus, the effect of change in absorptivity of cells is relatively less than that of solar panels.

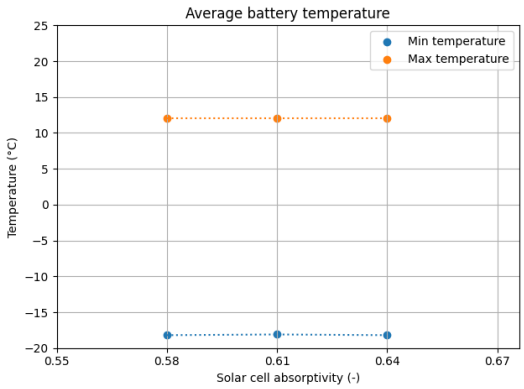

(a) Average Battery Temperature

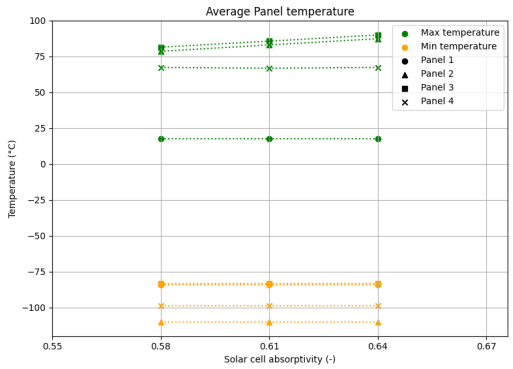

(b) Average temperature of individual solar cells on the 4 side panels

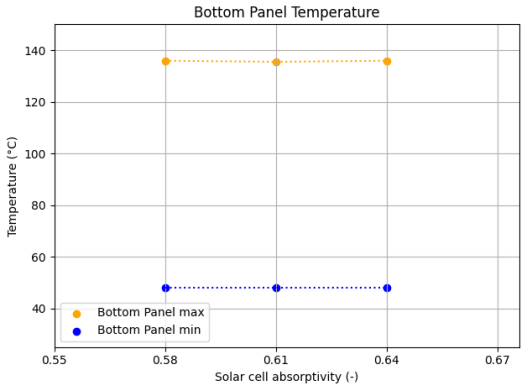

(c) Bottom Panel Average Temperature

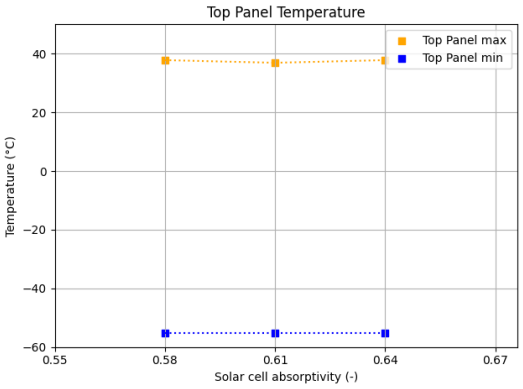

(d) Top Panel Average Temperature

Figure 4.5: Changes in temperatures with varying solar cell absorptivity

4.1.5. Solar cell emissivity

The solar cell emissivity is varied from 0.86 to 1.

The panel temperatures can be seen to decrease with increase in emissivity of the solar cells which is expected. Similar to the discussion for solar cell absorptivity, it does not affect the battery temperatures significantly.

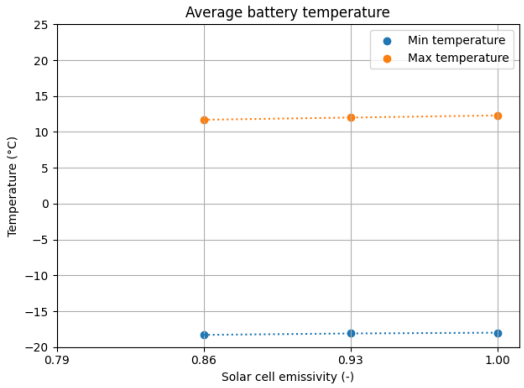

(a) Average Battery Temperature

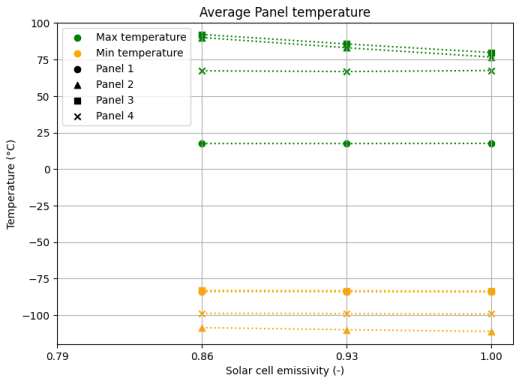

(b) Average temperature of individual solar cells on the 4 side panels

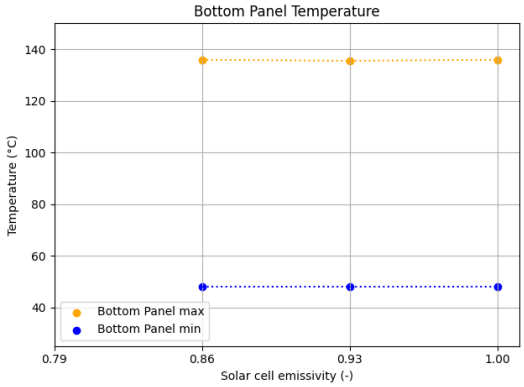

(c) Bottom Panel Average Temperature

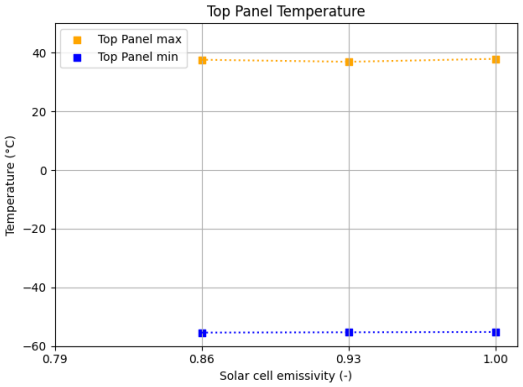

(d) Top Panel Average Temperature

Figure 4.6: Changes in temperatures with varying solar cell emissivity

4.1.6. PCB emissivity

The PCB emissivity is varied from 0.8 to 0.92.
The top and bottom panels are modeled as PCBs and the effect of increasing their emissivity is clearing visible as their temperatures reduce. Further, it is important to note that the battery temperatures do not vary much with changes in emissivity of PCBs which is a useful result for small satellite thermal modeling. Another way to infer this is that one cannot think of battery thermal control by relying on emissivity of PCBs.

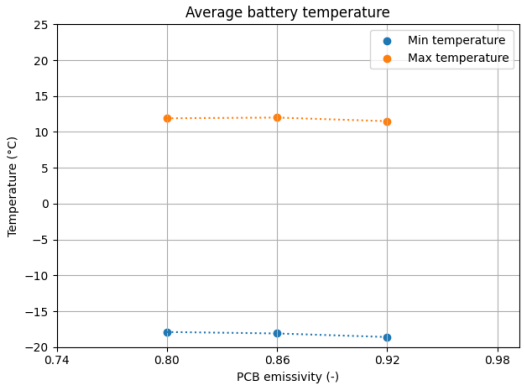

(a) Average Battery Temperature

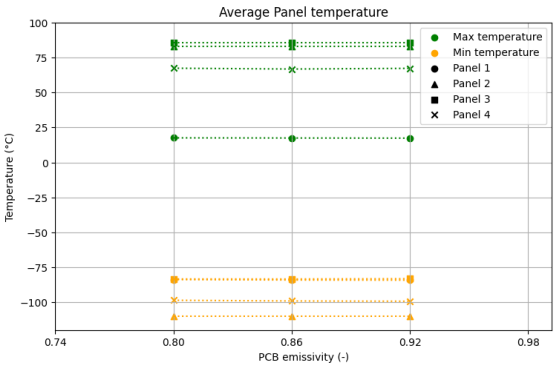

(b) Average temperature of individual solar cells on the 4 side panels

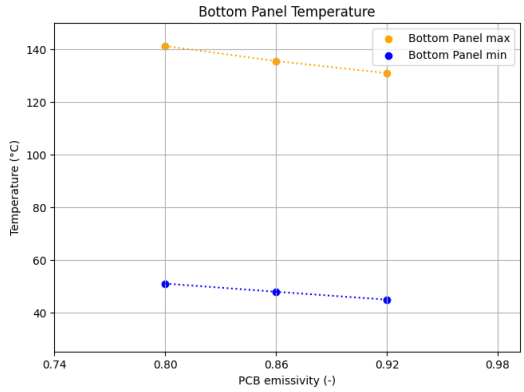

(c) Bottom Panel Average Temperature

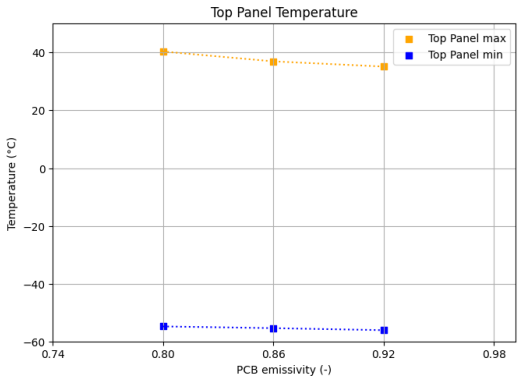

(d) Top Panel Average Temperature

Figure 4.7: Changes in temperatures with varying PCB emissivity

4.1.7. PCB heat capacity

The PCB heat capacity is varied from 510 J/kgK to 590 J/kgK.
The uncertainty in heat capacity of the PCBs does not affect the temperatures a lot which indicates that the uncertainty is not very high.

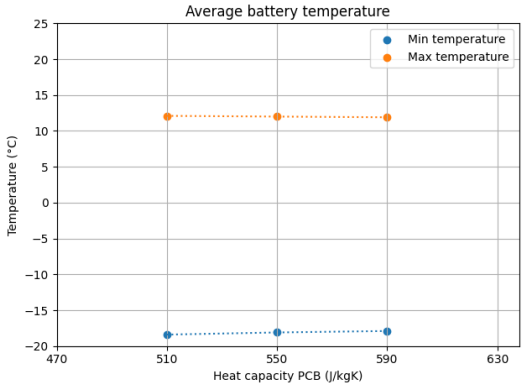

(a) Average Battery Temperature

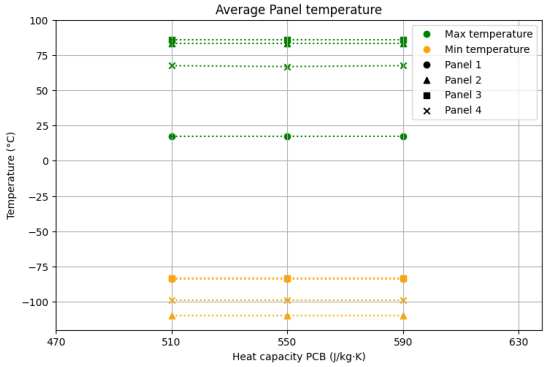

(b) Average temperature of individual solar cells on the 4 side panels

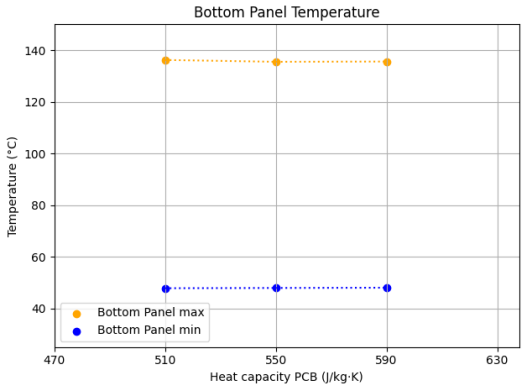

(c) Bottom Panel Average Temperature

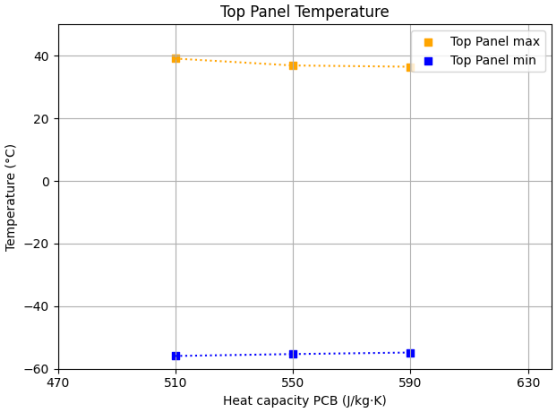

(d) Top Panel Average Temperature

Figure 4.8: Changes in temperatures with varying PCB heat capacity

4.2. Discussion

The sensitivity analysis performed gives us an insight into how the uncertainties of measured properties translate to the changes in average temperature of the battery, top and bottom panels, or the side panels.

To understand the effect of uncertainties, the maximum deviation observed in each: the battery, top, bottom and side panels is shown in figure 4.9 below.

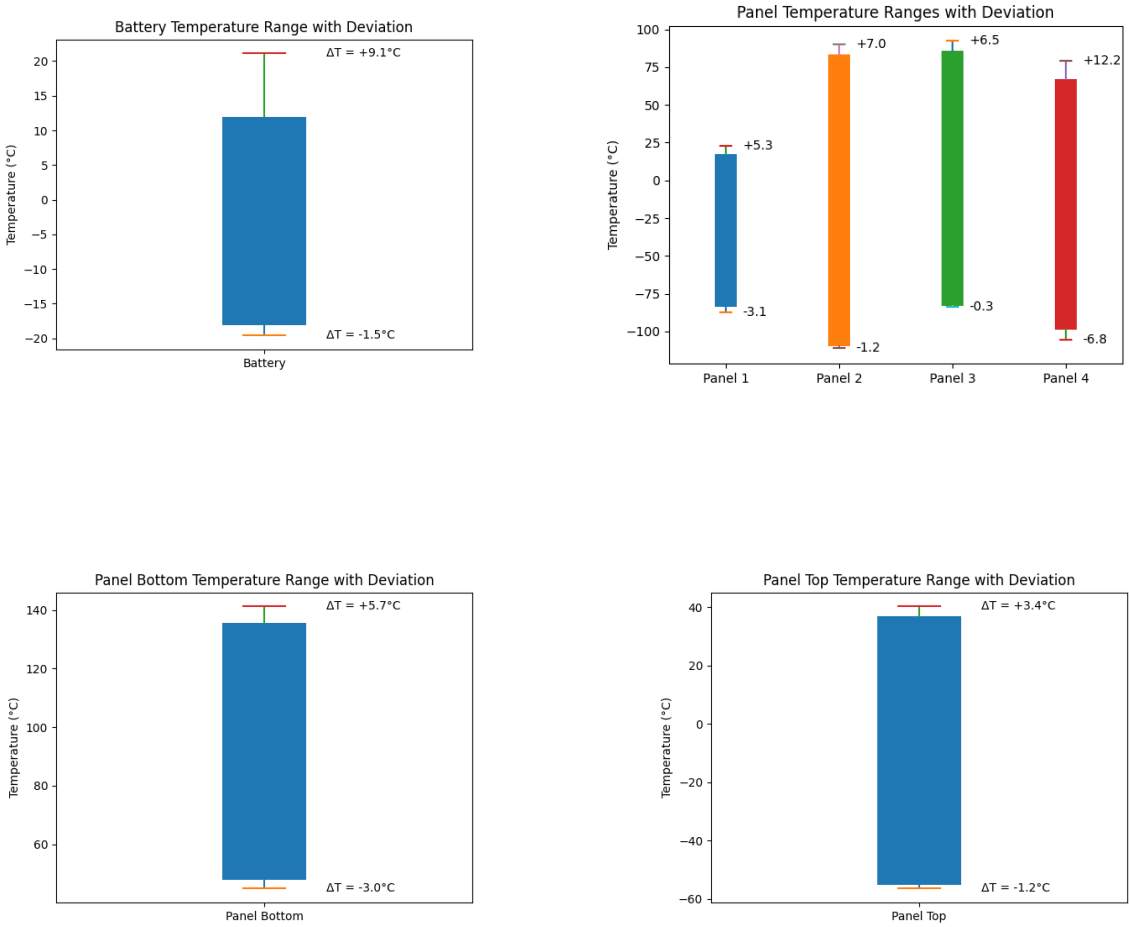

Figure 4.9: Temperature deviations due to uncertainties in property values obtained from experiments

Component	ΔT_{low} **(°C)**	ΔT_{high} **(°C)**
Battery	-1.5	+9.1
Panel Bottom	-3	+5.7
Panel Top	-1.2	+3.4
Side Panels (Max)	-6.8	+12.2

Table 4.3: Temperature deviations from nominal bounds

These values from table 4.3 can be combined with the operating temperatures given in table 4.1 to get a stricter temperature bound for which the thermal design should be done. The updated data has been shown in table 4.4.

Component	**Operating Range [°C]**	**Operating Range (after accounting for uncertainties) [°C]**
PCBs	-20 to +60	-18.5 to +51.9
Solar Cells	-100 to +100	-97 to +94.3
Battery	0 to +45	+6.8 to +32.8

Table 4.4: Component operating temperature ranges

Thus, we see that the battery sees the highest **percentage reduction** in the operating range **by** approximately **42%**, which further highlights it being a thermally critical component.

5

Reduced Modeling

This chapter talks about the detailed calculation of linear conductance across the spacer-PCB stack and this also involves the creation of a reduced thermal model for the PCB.

Spacers are structural components that are placed along threaded rods to separate PCBs and other components in a CubeSat stack.
Connectors are components which link the PCBs to share data and power.

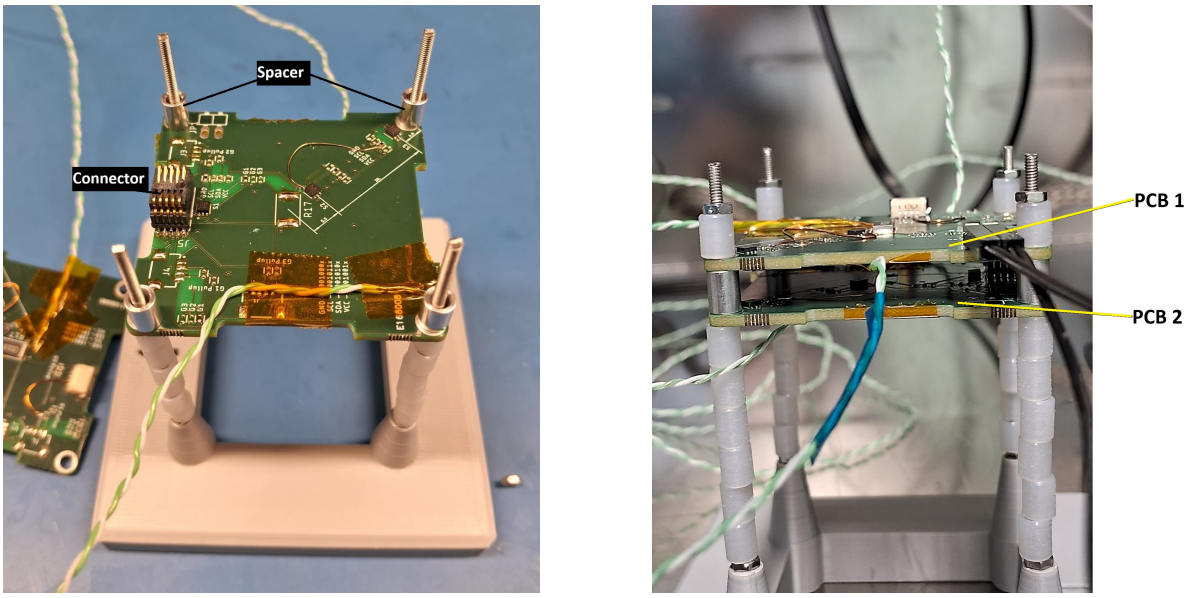

Figure 5.1: Spacer and connector in a PCB stack

Heat transfer between the two PCBs occurs through both radiation and conduction via the spacers. To accurately model this behavior, it is essential to determine the effective thermal conductance across the PCB-spacer-PCB stack.

This chapter outlines the methodology used to evaluate this conductance, along with the results obtained and their validation.

To provide a brief overview, the experimental setup consists of two PCBs separated by spacers and a connector with a height of 6 mm, as shown in Figure 5.1. The upper PCB is equipped with a centrally located heater, while the lower PCB remains unheated. The **objective** is to **quantify the heat transferred through the spacers**. This is achieved by:

- Determining the fraction of input heat that remains within the PCB–spacer–PCB system, accounting for losses through the power supply cable.
- Measuring the total heat received by the unheated PCB. This is done by determining how much heat the unheated PCB loses via radiation to its surroundings in steady state.
- Estimating the heat transfer due to radiation between the two PCBs.
- Finally, the total heat transfer through the spacer can be given by total heat received by unheated PCB minus the heat it received via radiation.

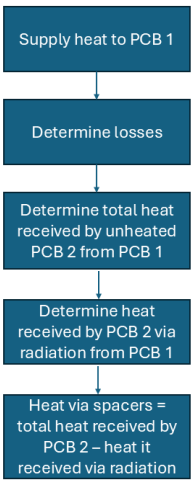

Figure 5.2: Procedure for determination of heat transfer through spacers

Before proceeding with these calculations, two key factors were investigated:

- The influence of spacer torque on heat transfer between the PCBs.
- The significance of radiative heat transfer in the overall thermal exchange.

To study these aspects, thermal balance experiments were conducted in which the torque applied to the spacers was varied, and Multi-Layer Insulation (MLI) was introduced in selected tests.

From the next section onward, the **top PCB** with the central heater will be referred to as **PCB 1** while the **bottom PCB** without the heater will be referred to as **PCB 2**.

5.1. Preliminary Thermal balance tests

These are tests performed for the stack to understand the effect of torque and contribution of radiation in heat transfer between the two PCBs.

PCB 1 has an inbuilt heater and four temperature sensors; while thermocouples were attached on PCB 2 as shown in figure 5.3.

Figure 5.3: PCB 1 and PCB 2

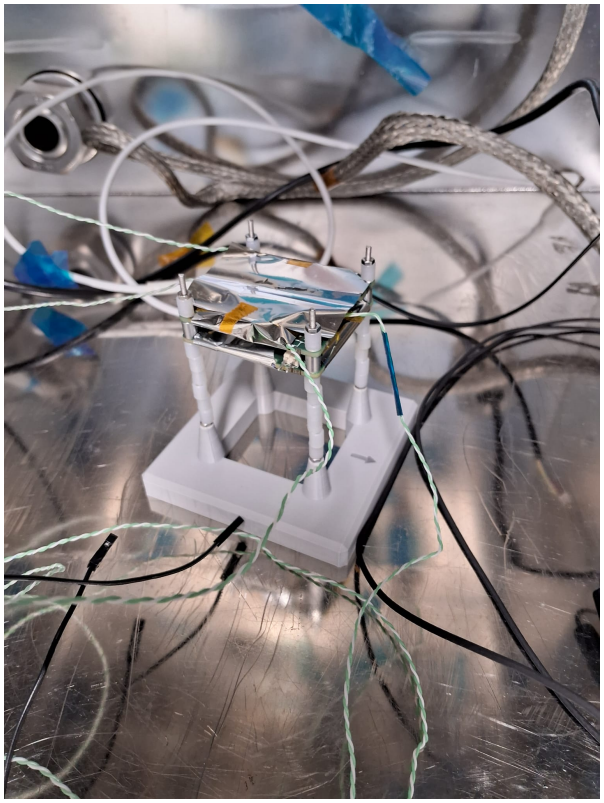

Figure 5.4: Test setup with MLI

For these preliminary tests, 1 W of power was supplied to PCB 1 and the temperature distribution of both boards was recorded.

For understanding the significance of radiation heat transfer, the test was repeated with (figure 5.4) and without MLI at the same input power.

For considering the effect of torque, 3 cases were considered: hand torque, 0.04 Nm and 0.1 Nm (No MLI was used for these tests).

The conclusions have been summarized in the tables 5.1 and 5.2 below. Reference Value refers to the distribution of temperatures on the board surfaces for the Test 1.

Table 5.1: Effect of spacer torque on temperature distribution along PCB surfaces

Test	Torque	Temperature Distribution
Test 1	0.1 Nm	Reference value
Test 2	0.04 Nm	Same as reference
Test 3	Hand torque	Same as reference

Table 5.2: Effect of MLI on temperature distribution along PCB surfaces

Test	MLI	Temperature Distribution
Test 1	No	Reference value
Test 2	Yes	Increase of approximately 20°C

These experiments showed that the **temperature distribution is independent of spacer torque**, while **radiative heat transfer is significant and must be considered**. Additionally, they provided a better understanding into the thermal behavior of the system, allowing us to make a better choice for

thermocouple placement and the expected time required to reach steady-state conditions.

An **important thing to note** is that the location on the PCBs where the spacers are placed contain **tin coating** on the surface. This could be one of the explanations for why there is no change in temperature distribution with change in torque because tin, being malleable at room temperature, will deform under higher torque and thus the effect of increased torque would not be very prominent. It is important to repeat these tests on actual components if tin is not going to be present in the actual flight PCBs.

A very important parameter which was deciding the torque value, is now out of the picture. Also, based on these experiments, it was decided to model each PCB as a 3x3 grid in ESATAN and the code. This decision was based on the number of available thermocouples and the temperature variation observed from the center of the PCB towards the corner for a power of 1 W (maximum power in any future tests).

5.2. Single PCB-1 test

In the tests described in the previous section, one of the tests had a thermocouple attached to PCB 1 despite it already having in-built temperature sensors. This was done out of curiosity to check the temperature value at a location which was radially at the same distance from the central heater as one of the in-built temperature sensors. Well, the only difference was the copper layout underneath the uniform paint layer of the PCB, which is what triggered the curiosity.

The results were unexpected. The path to the thermocouple from the heater had more copper but still showed a temperature value smaller than that of the in-build temperature sensor.

The difference was within the thermocouple accuracy of ± 2.2 K, but just to do a check it was decided to place thermocouples next to all the in-built temperature sensors to see if they measure the same values.

The results have been shown in figure 5.5. The red color represents copper, and blue represents FR4. The entire PCB has a top layer of paint which is not shown here. The figure shows the data of temperature measurements in degree celsius for two different input powers.

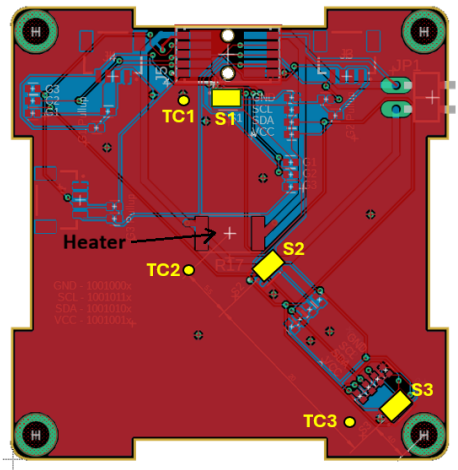

TC – represents thermocouples
S – represents in-built heaters

Input Power 1		Input Power 2	
TC1	S1	TC1	S1
42.7°	47.5°	29.5°	31.4°
TC2	S2	TC2	S2
43.6°	47.9°	30°	31.6°
TC3	S3	TC3	S3
40.1°	41.7°	28.9°	29°

Figure 5.5: Thermocouple vs in-built temperature sensor readings

The figure 5.5 shows that all thermocouples measure a value slightly lower than the in-built temperature sensors. This could be due to multiple reasons:

- All the thermocouples were detached slightly.
- The thermocouples have a constant offset

- The in-built temperature sensors are directly connected to the copper layer underneath along which most of the heat flows. And the thermocouples are attached to the paint layer on top.

Out of the three reasons mentioned above, the first can be disregarded because a similar behavior was observed in the previous preliminary test.
The second reason can also be disregarded because the initial room temperature measured by the thermocouple and in-built temperature sensors was the same and also the difference between values seen in figure 5.5 is not constant.

The third reason makes sense as the the heat flow from the copper layer to the outer surface happens across the paint layer which has a low thermal conductivity, thus the temperature difference would not be negligible which is what the thermocouples pick up.

In other words, the in-built sensors are reading temperature values directly from the copper layer beneath the paint layer, while the thermocouples pick up readings from the paint layer. It further makes sense to see that the difference is negligible close to the corners of the PCBs because majority of the heat has already been transferred from the copper layer to the top layers by the time it reaches the corners.

This implies that to model radiation between two PCBs in the stack, thermocouples will have to be used on both PCB 1 and 2.

5.3. Heat Loss determination

Four tests were done on PCB-1 at different input powers to determine the surface temperature distribution and using that determine the heat loss along the cables.

The thermocouples would map the surface of the PCB. And during steady state of the thermal balance test the power input will be equal to heat loss by radiation and heat loss along the cables. The heat loss by radiation can be calculated because the emissivity value has been measured as discussed in section 3.3.

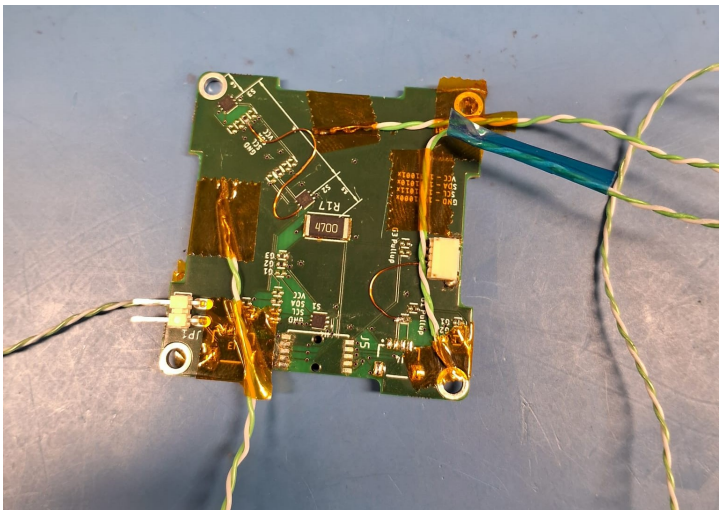

Figure 5.6: Thermocouple placements for heat loss test

Table 5.3: Heat loss determination

Power Input (W)	Radiation (W)	Cable Loss (W)
0.296	0.212	0.084
0.488	0.360	0.128
0.729	0.526	0.203
1.000	0.690	0.310

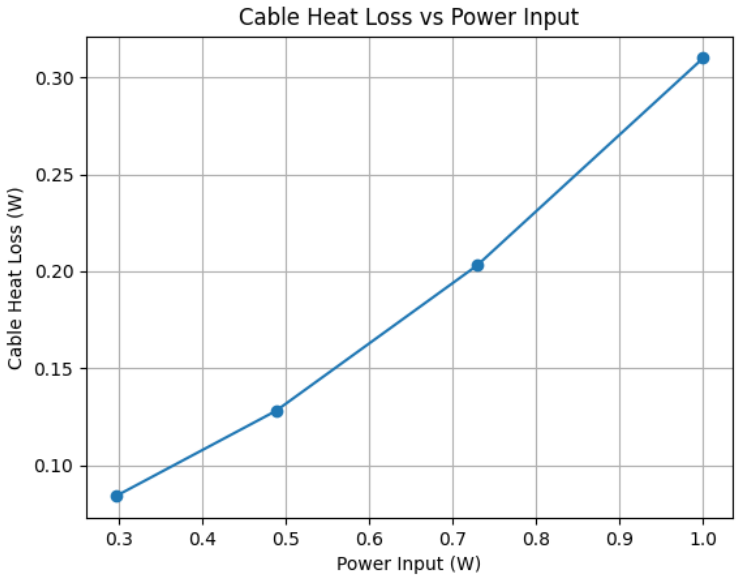

Figure 5.7: Heat loss along cable vs power input

The above curve can be defined using equation:

$$Q_{\text{heat loss}} = 0.1737P_{\text{in}}^2 + 0.0963P_{\text{in}} + 0.0401 \tag{5.1}$$

5.4. Tests for determination of spacers and connector combined linear conductance

Now, after the knowledge gathered from previous tests about heat loss, effect of spacer torque and significance of radiation heat transfer between PCBs, the test for the PCB-spacer-PCB stack can be conducted. Note that the connector will also be included and an equivalent linear conductance between the two PCBs will be calculated.

Based on the previous discussion (section 5.1) about dividing the PCB into 3 x 3 grid, each PCB has been represented by 2 surfaces of a 3 x 3 grid as shown in the figure 5.8.

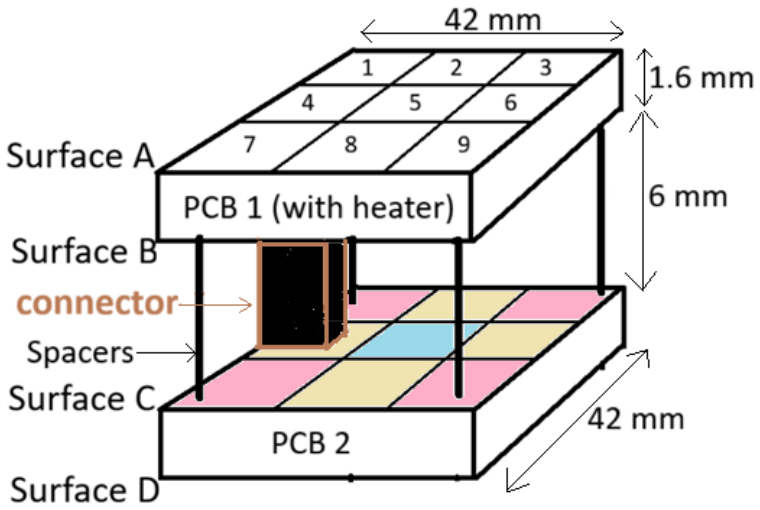

Figure 5.8: Representation of spacer and connector linear conductance test

By **symmetry**, it is assumed that **temperature** of nodes 2, 4, 6 & 8 is the **same** and also the temperatures of nodes 1, 3, 7 & 9 is the same as seen from the **colors** in figure 5.8.

Thus, each surface requires 3 measurements at the most.

Since there were only four thermocouples, each test was repeated twice after changing the thermocouple locations. Thermocouples (highlighted in yellow) were places at the following locations shown in figure 5.9.

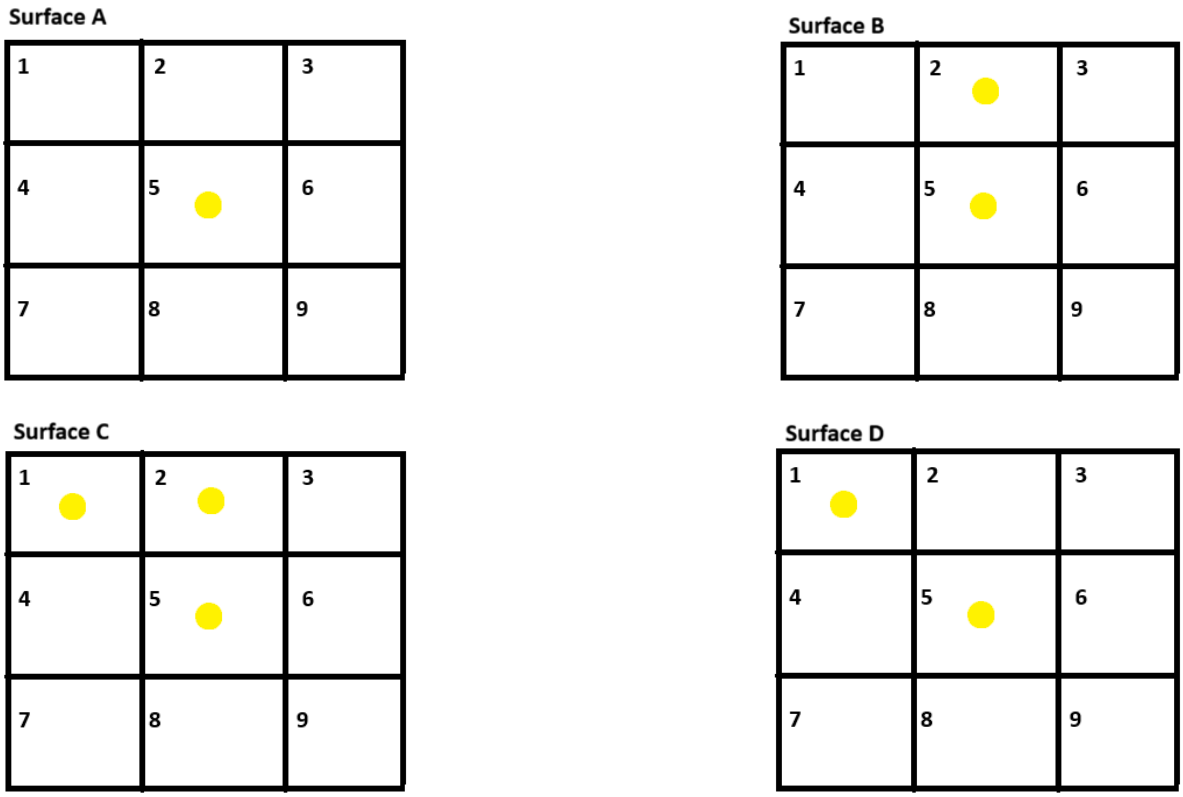

Figure 5.9: Thermocouple location on each surface

Power is supplied to the heater and the test is conducted within the enclosure (ϵ_{IR} = 0.8) inside the vacuum chamber.

The setup was modeled in ESATAN to obtain the radiative exchange factors between the PCBs and the PCB-enclosure faces. This data was stored in an excel sheet and based on the temperatures obtained from the thermal balance test, the radiation heat transfer was determined.

During steady state, PCB 2 receives heat via radiation from surface B to C and via the spacers and connector. This exact amount of heat is lost via radiation from surface C and D of PCB 2 to the walls of enclosure which is at room temperature as shown in figure 5.10. Where, the red color signifies heat input to PCB 2, while green color signifies heat loss to surrounds via PCB 2. Both of which will be equal in steady state.

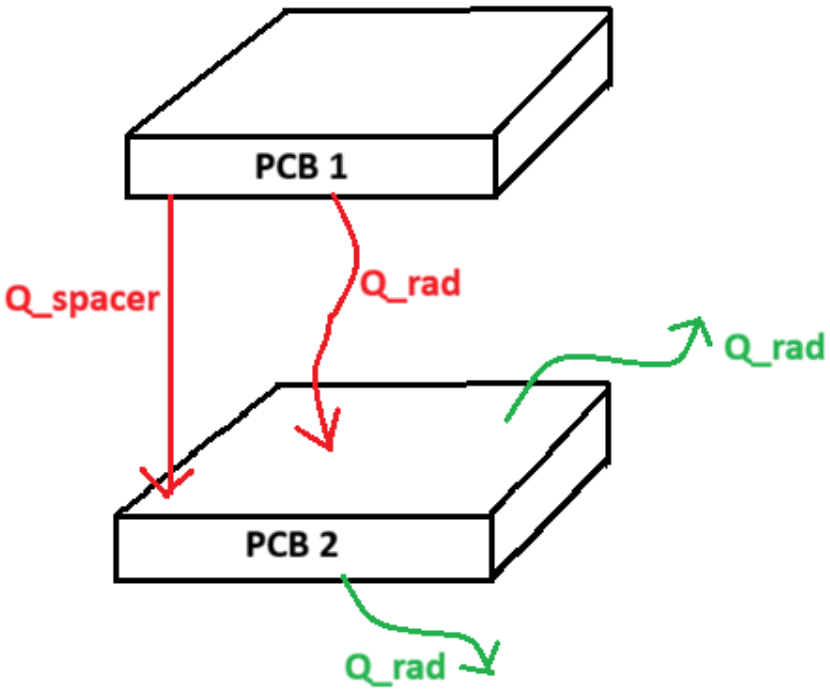

Figure 5.10: Steady state condition

The only unknown is the heat transfer via the spacers and connector which can be found from the steady state scenario.

Further, the temperature difference across the spacers is known which can be used to determine the linear conductance (GL_{spacer}):

$$GL_{spacer} = Q_{spacer}/\Delta T_{spacer}$$

Note that the use of word spacer implies all the four spacers and one connector together.

Table 5.4 shows the results obtained from the test at a power input of 1W.

Table 5.4: Test results for GL spacer

Parameter	Value
P_{in}	1 W
Heat loss	0.31 W
Total heat received by PCB2	0.266 W
Radiation (Surface B to C)	0.09 W
ΔT_{spacer}	4.1 °C
Q_{spacer}	$0.266 - 0.09 = 0.176$ W

$$GL_{spacer} = \frac{Q_{\text{spacer}}}{\Delta T_{\text{spacer}}} = \frac{0.176}{4.1} \text{ W/K} = 0.04 \text{ W/K}$$

This is the equivalent value, which would translate to 0.01 W/K per spacer.

Note that after consideration of error propagation from thermocouple and emissivity accuracy, the linear conductance varies from **0.01 to 0.1 W/K** for all spacers and connector combined. Thus, the value of 0.05 W/K **(=0.0125 W/K per spacer)** will be used for the reduced model discussed in the next section.

5.5. Reduced Model for PCB-spacer-PCB stack

With all the information obtained so far from the work of this thesis, a reduced thermal model has been developed to predict the steady state temperatures of two stacked PCBs.

- An ESATAN Model has been developed for the same, but this assumes the PCBs to be 2D shells, which means each PCB has the same temperature at the top and bottom surface.
- Also, a calculator has been developed in MS Excel that determines the temperature of the 9 nodes for all 4 surfaces shown in figure 5.8.

5.5.1. Calculator

The calculator uses the heat loss from equation 5.1 and radiative exchange factors with the enclosure (ϵ_{IR}=0.8) from ESATAN.

Then, the temperatures of PCB 1 (heating board) have been obtained by interpolation of experimental results for different input powers.

In the next step, the radiative exchange factors and GL_{spacer} value is used to determine the temperatures of PCB 2.

The excel sheet will be added to the repository as a supplementary document with this thesis.

5.5.2. ESATAN Reduced Model

The PCBs are modeled as shells and the spacers as non geometric thermal nodes.

The bulk and optical properties used for the model have been shown in the table below. All the values are the experimentally determined values from previous tests.

Table 5.5: Material and thermal properties

Component	Property	Value
PCB	Thermal conductivity (k)	15 W/mK
PCB	Specific heat capacity (C_p)	550 J/kgK
PCB	Emissivity (ε)	0.92
Enclosure	Emissivity (ε)	0.8
Spacer (X4)	GL_{spacer}	0.0125 W/K per spacer

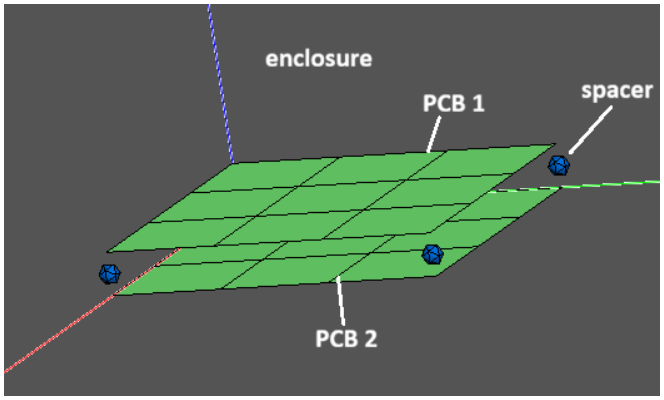

Figure 5.11: Reduced thermal model in ESATAN

The central node of one PCB is given a fixed boundary condition of total area heat load and the value is calculated after accounting for heat loss determined using equation 5.1.

5.6. Comparison of experimental data with results of the calculator and the ESATAN reduced thermal model.

This section will show the outputs obtained from the tests data and compare it with the values obtained the calculator and ESATAN Model for 1 W, 0.488 W and 0.296 W of input power.

Cells with the same color indicate the same temperatures.

5.6.1. Results at P_{in} = 1 W

A

45.5	48	
	48	

B

45.5	48.8	
	50.8	

C

40.4	40	
	42.9	

D

37.4	37.4	
	37.4	

Figure 5.12: Experimental results (temperature values in °C) for P_{in} = 1 W

A

46.1	48.2	
	49.3	

B

46.1	49.3	
	52.5	

C

41.3	41.3	
	41.3	

D

37.0	37.0	
	37.0	

Figure 5.13: Calculator results(temperature values in °C) for P_{in} = 1 W

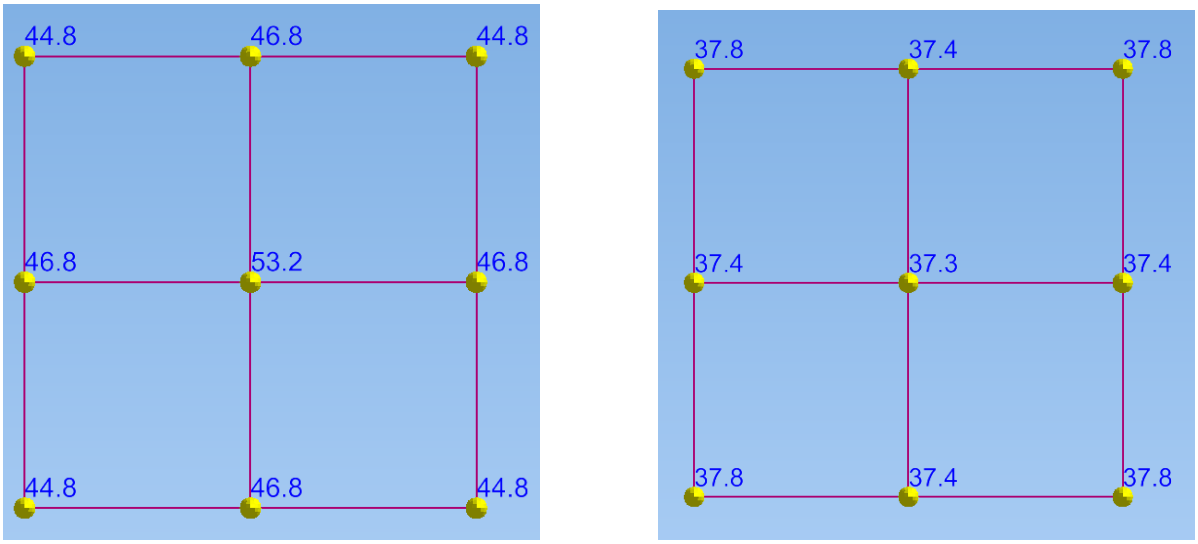

(a) PCB 1 **(b)** PCB 2

Figure 5.14: ESATAN results(temperature values in °C) for $P_{\text{in}} = 1$ W

If we make a node to node comparison, the calculator has a maximum deviation of 1.7°C. It predicts the maximum temperature to be 1.7°C higher than that achieved and the lowest temperature 0.4°C lower than that achieved.
The ESATAN model predicts the highest temperature near the heater to be 2.4°C higher than the experimental results.

5.6.2. Results at P_{in} = 0.488 W and 0.296 W

For 0.488 W, the calculator has a maximum deviation of 3.3°C. Here , the calculator predicts maximum temperature to be 1.2°C higher and the lowest temperature to be 0.7°C lower. This allows for a conservative estimate.

The ESATAN results also make a conservative estimate by extending the maximum and minimum temperatures by +1.5°C and -0.5°C respectively.

The experimental results obtained for 0.296 W are around 2°C higher than the calculator and ESATAN results.

5.7. Discussion

Three experimental values were compared with the results of the calculator and ESATAN and show a good match as discussed earlier. The key takeaway from this chapter is **value of the** GL_{spacer} **obtained** and the **procedure of creation of a reduced model** which can be updated to be used for a PCB stack inside an enclosure the size of a CubeSat. This can be done by **updating** the **radiative exchange factors** and conducting experiments to determine the **new equation for power loss** along cables which will change because the internal temperatures will change for same given input power as the enclosure will be much smaller.

6

Conclusion and Future Work

At the end we look at the Research question again:

How can an integrated framework, that combines experimental determination of thermo-optical properties with reduced-order thermal modeling, be developed to quantify the accuracy of preliminary thermal modeling for smallsat teams?

This can be broken down into the following sub-questions:

1. How can experimentally obtained thermo-optical property data be compiled into a reliable database for CubeSat materials?
2. How can reduced-order thermal models be generated by using the database?
3. How can the reduced-order thermal sub-models be compared to experimental data?

6.1. Conclusions

This thesis addressed the challenge of performing reliable thermal analysis for CubeSats by developing an integrated framework that combined experimental data with reduced-order thermal modeling. The motivation stemmed from the limitations faced by student teams like lack of accurate material property data, lack of time and expertise for thermal simulations.

With regard to the first research sub-question, a series of experiments were designed and performed to obtain thermal conductivity, heat capacity, infrared emissivity and solar absorptivity for key components like solar cells, panels and PCBs. The results included nominal values with uncertainties which is often not given in literature. The uncertainties were further used to perform a sensitivity analysis that help us determine the error in temperature predictions.

With regard to the second and third research sub-question, a specific reduced-order thermal model was created for a two PCB stack within an enclosure. Initially, the equivalent linear conductance across the spacer and connector was determined. This was found to be independent of the torque value applied on the spacers. Further, the heat transfer via radiation between the PCBs was found to be significant as the usage of MLI led to a 40% increase in board temperatures. This was against the initial hypothesis which assumed that radiation heat transfer would have a smaller impact.

Further, a reduced-order model in ESATAN made use of thermo-optical properties obtained for the PCB along with the linear conductance across the spacers. This was compared with experimental results which showed a good match with errors within 2.5°C of the experimental values.

It is important to note that the reduced model is for a specific case of a stack within an enclosure. The methodology that led to the creation of the reduced model could be replicated to understand the heat

transfer between stacks within solar panels instead of the enclosure. This would require determination of a new heat loss equation for losses though power supply wires and new radiative exchange factors.

Overall, the combination of validated material properties and procedure to generate reduced-order thermal models could help student teams make better thermal estimates during the initial design phases.

6.2. Future Work

Regarding modeling, the battery properties and contact conductance values provided in the current model needs to validated experimentally. This is required to make better temperature predictions from the model. Also, the PCB is currently modeled as a 2D shell, it can be updated to a 3D solid to account for heat flow through the thickness. This can be done by placing a tape heater on one side of the PCB and measuring temperatures on both sides using thermocouples. Here, the heat loss characteristics can be used as described in section 3.2.

Regarding the design of experiments, the in-built temperature sensors on the PCB need to be modified to be able to measure the surface temperature instead of the temperature of the copper layer which they currently do. This is needed for better modeling of radiation exchange. J-type thermocouples should be used as they have a better accuracy ($\pm$1 K) than the k-type ($\pm$2.2 K) being used currently. Tests should be repeated on similar components (solar cells, panels and PCBs) from different production batches to understand the difference, if any. Currently, kapton tape is being used for sticking the thermocouples. This leads to detachment of sensors at times, especially at temperatures close to 100°C. This can be replaced with RTV glue. Delfi-PQ used PCBs instead of solar panels in the Z direction of the pocketqube. Thus, the solar absorptivity of PCBs should be measured using the spectrophotometer available at the Applied Sciences faculty.

Regarding the sensitivity analysis, the effect of linear conductance can be included now that we have an effective value ranging from 0.01 W/K to 0.1 W/K.

Regarding the reduced modeling, the current PCBs had very minimal components on their surfaces. A few components should be introduced over the board and the change in temperatures and heat transfer should be noted using thermocouples. If significant changes are observed, then models should be created to account for the added heat capacity of the new components. As discussed earlier, the two PCB stack case with an enclosure should be updated with an enclosure that represents the solar panels (in other words, update the radiative exchange factors). This can be used to model an actual stack inside a CubeSat.

References

[1] Ak. te. and R.C. van. *NLR-Royal Netherlands Aerospace Centre Thermal Modelling of CubeSats in ESATAN-TMS: A Modular Approach An ICES2020 Conference Proceeding*. Tech. rep. 2020. URL: www.nlr.nl.

[2] Abdulaziz Alanazi and Jeremy Straub. "Engineering methodology for student-driven CubeSats". In: *Aerospace* 6.5 (May 2019). ISSN: 22264310. DOI: 10.3390/AEROSPACE6050054.

[3] Ziqi Zhang and Stefano Speretta. *Orbital Temperature Model Construction for Delfi-PQ*. Tech. rep. URL: https://www.n2yo.com/satellite/?s=51074,.

[4] Juan Perales Gómez. "Thermal Analysis, Design and Verification of an Academic CubeSat Mission in a MBSE Context". In: (2024).

[5] André G C Guerra, Diego Nodar-López, and Ricardo Tubó-Pardavila. "Thermal analysis of the electronics of a CubeSat mission". In: *arXiv* (2018).

[6] Hiroshi Kato, Makiko Ando, and Moriyasu Fukuzoe. "Toward Uncertainty Quantification in Satellite Thermal Design". In: *Transactions of the japan society for aeronautical and space sciences, aerospace technology japan* 17.2 (2019), pp. 134–141. ISSN: 1884-0485. DOI: 10.2322/TASTJ.17.134.

[7] F S Meijering. "Modular Thermal Analysis for CubeSats and PocketQubes". PhD thesis. TU Delft, 2024. URL: http://repository.tudelft.nl/..

[8] R Ávila De Luis. *Standardized Thermal Control Solutions for Pocketcubes*. Tech. rep. URL: http://repository.tudelft.nl/.

[9] K. Azar and J. E. Graebner. "Experimental determination of thermal conductivity of printed wiring boards". In: *Annual IEEE Semiconductor Thermal Measurement and Management Symposium* (1996), pp. 169–182. ISSN: 10652221. DOI: 10.1109/stherm.1996.545107. URL: https://ieeexplore.ieee.org/document/545107.

[10] C Macco. *Design and Verification of the Delfi-n3Xt Thermal Control Subsystem*. Tech. rep. 2014.

[11] Lionel Jacques. *Thermal Design of the Oufti-1 nanosatellite*. Tech. rep. 2009. URL: https://www.researchgate.net/publication/265217275.

[12] M M Finckenor and R F Coker. "Optical Properties of Nanosatellite Hardware". In: (2014).

[13] V N Gorev et al. "The effect of the PCB solder mask type of the hull outer surface of the CubeSat 3U on its thermal regime". In: IOP, 2020. DOI: 10.1088/1757-899X/734/1/012027.

[14] *Solar Cell Coverglasses*. Tech. rep. QiOptiq. URL: https://www.excelitas.com/file-download/download/public/58456?filename=Qioptiq_Space-Qualified_Cover_Glass_Datasheet.pdf.

[15] *Azur Space: Triple Junction GaAs Solar Cell*. Tech. rep. 2016. URL: https://www.azurspace.com/images/products/0003401-01-01_DB_3G30A.pdf.

[16] *ECSS-E-ST-31C - Space engineering*. Tech. rep. Nov. 2008.

[17] David Gilmore. *Spacecraft Thermal Control Handbook, Volume I: Fundamental Technologies*. American Institute of Aeronautics and Astronautics, Inc., Dec. 2002. DOI: 10.2514/4.989117. URL: https://arc.aiaa.org/doi/book/10.2514/4.989117.

[18] I. Savija et al. "Review of thermal conductance models for joints incorporating enhancement materials". In: *Journal of Thermophysics and Heat Transfer* 17.1 (2003), pp. 43–52. ISSN: 15336808. DOI: 10.2514/2.6732.

[19] Daniel J Mckinzie. *SIMPLIFIED METHOD FOR CALCULATING THERMAL CONDUCTANCE OF ROUGH, NOMINALLY FLAT SURFACES I N HIGH VACUUM*. Tech. rep. URL: https://ntrs.nasa.gov/citations/19700007806.

[20] ALBIN K J. HASSELSTRÖM and U. ESKIL NILSSON. “Thermal Contact Conductance of bolted joints”. In: (2012). URL: https://publications.lib.chalmers.se/records/fulltext/159027.pdf.

[21] Philipp B Hager et al. *Contact Conductance in Common CubeSat Stacks*. Tech. rep. 2019.

[22] Matteo Quirino et al. “Validation of the Thermal Model for the HERMES CubeSat Payload and Evaluation of the Performance of Newly Designed Passive Thermal Links”. In: *Aerotecnica Missili & Spazio* (Sept. 2025). ISSN: 0365-7442. DOI: 10.1007/s42496-025-00287-z.

[23] M. Michael Yovanovich. “Four decades of research on thermal contact, gap, and joint resistance in microelectronics”. In: *IEEE Transactions on Components and Packaging Technologies* 28.2 (June 2005), pp. 182–206. ISSN: 15213331. DOI: 10.1109/TCAPT.2005.848483.

[24] M. G. Cooper, B. B. Mikic, and M. M. Yovanovich. “Thermal contact conductance”. In: *International Journal of Heat and Mass Transfer* 12.3 (1969), pp. 279–300. ISSN: 00179310. DOI: 10.1016/0017-9310(69)90011-8.

[25] *ECSS-E-HB-32-23A - Space Engineering*. Tech. rep. 2010.

[26] A K Te Nijenhuis et al. “Thermal Analysis and Verification of CubeSat Designs with ESATAN-TMS”. In: *50th International Conference on Environmental Systems*. Vol. 104. 2021, pp. 12–15.

[27] Lonny Kauder. *Spacecraft Thermal Control Coatings References*. Tech. rep. NASA, Dec. 2005. URL: http://www.sti.nasa.gov/STI-homepage.html.

[28] *Space product assurance Measurements of thermo-optical properties of thermal control materials ECSS Secretariat ESA-ESTEC Requirements & Standards Division Noordwijk, The Netherlands*. Tech. rep. 2008.

[29] Mustafa Sivasligil et al. “Infrared emissivity measurement approach for solid and opaque materials”. In: *Applied Optics, Vol. 64, Issue 10, pp. 2525-2533* 64.10 (Apr. 2025), pp. 2525–2533. ISSN: 2155-3165. DOI: 10.1364/AO.550393.

[30] Gary Orlove. “Two Dimensional Spatial Emissivity Correction Technique”. In: (2011).

[31] Trieu Khoa Nguyen and Bach Phuong Ho Thi. “A simple method for determining surface emissivity to improve infrared camera temperature measurements”. In: *Measurement Science and Technology* 36.8 (Aug. 2025). ISSN: 13616501. DOI: 10.1088/1361-6501/ADFC8F.

[32] M. Vellvehi et al. “Irradiance-based emissivity correction in infrared thermography for electronic applications”. In: *Review of Scientific Instruments* 82.11 (Nov. 2011). ISSN: 00346748. DOI: 10.1063/1.3657154.

[33] Gabriella Rossi et al. “New spectrally selective coatings for CSP linear receivers operating in air at high temperature”. In: *Applied Research* 3.2 (Apr. 2024), e202200117. ISSN: 27024288. DOI: 10.1002/APPL.202200117;PAGE:STRING:ARTICLE/CHAPTER.

[34] *Guide for Infrared Spectroscopy*. Tech. rep. BRUKER Optics.

[35] Christian A. Gueymard. “Revised composite extraterrestrial spectrum based on recent solar irradiance observations”. In: *Solar Energy* 169 (July 2018), pp. 434–440. ISSN: 0038-092X. DOI: 10.1016/J.SOLENER.2018.04.067. URL: https://www.sciencedirect.com/science/article/pii/S0038092X1830433X?via%3Dihub.

[36] Daniel Rønning and Yinglu Tang. “Irradiation resistance of thermo-optical properties of zirconium diboride by 3 MeV electrons”. In: *Frontiers in Space Technologies* 5 (Mar. 2024), p. 1355258. DOI: 10.3389/frspt.2024.1355258.

[37] *Lab IR paint*. URL: https://paints.labir.cz/en/paints/herp-ht/.

A

Solar Absorptivity

A.1. Test Procedure

1. Clean sample with alcohol wipe and let it dry for about 30 minutes.
2. Start the spectrometer and let it sit idle for 10 minutes (the time it takes for lamp to heat up).
3. The clip type sample holder should be set to 8 degrees as the angle of incidence. This is the recommendation by the technician (the manuals and reports near the machine state that the calibration has been done at this angle).
4. Place holder inside integrating sphere and ensure the wavelength range and step size is set as desired in the software.
5. Press the autozero button. This is to measure the background.
6. Place the sample in the sample holder and ensure the angle of incidence does not change while doing so (holder is a bit sensitive and the angle of incidence can change because of sudden movements).
7. Run the scan and save data.
8. Repeat test 3 times for each component.

A.2. Sample calculation

The sample calculation shown below is for a sample of ceramic (ZrB2). This was chosen as a reference to verify the calculation procedure as the solar absorptivity value of a similar sample has been obtained earlier[36].

Step 1:

Solar irradiance data E_λ is obtained as shown in figure A.1.

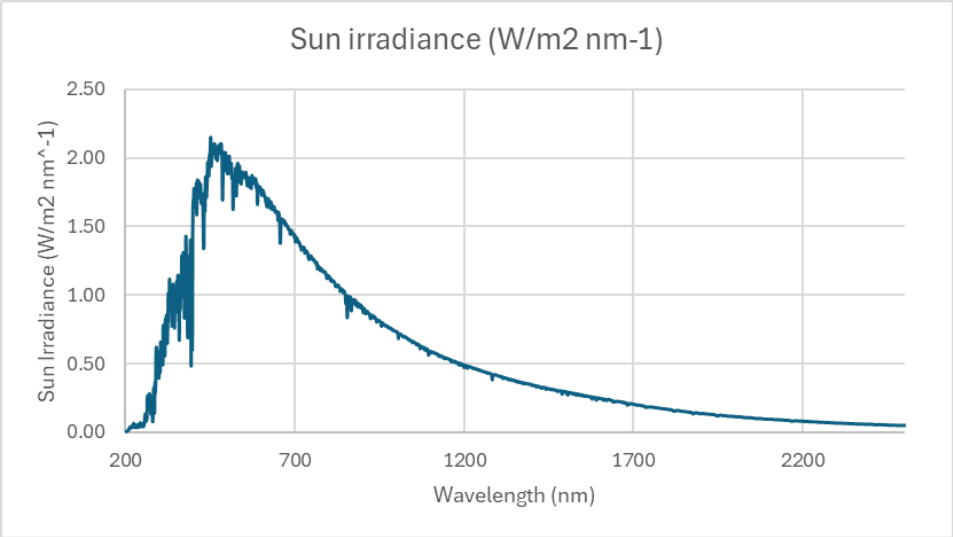

Figure A.1: Solar Irradiance
[35]

Step 2:
Absorbance (A(λ)) of sample obtained from spectrometer.

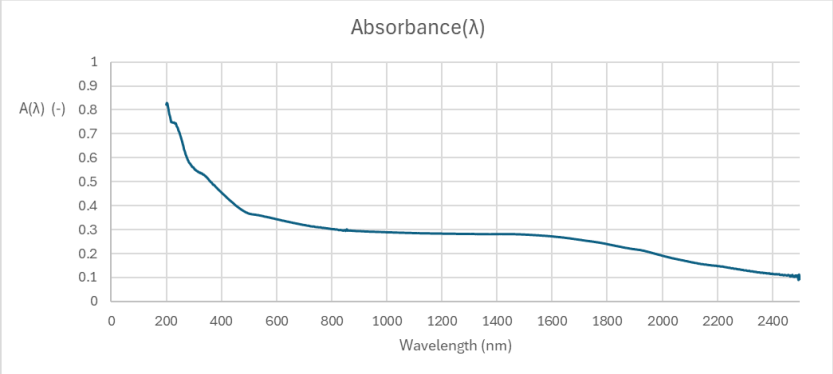

Figure A.2: Absorbance as a function of wavelength

Step 3:
Alpha is obtained using the mathematical manipulation explained in section 3.1.1

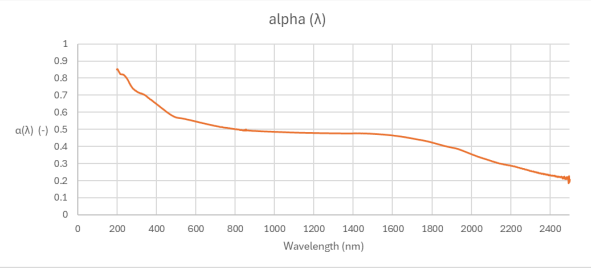

Figure A.3: Solar absorptivity as a function of wavelength

Step 4:
Now using equation 3.6,

$$\alpha_s = \frac{\sum \alpha(\lambda)\, E_\lambda}{\sum E_\lambda}$$

$$\alpha_s = 0.529$$

B

Heat Loss Test

B.1. Test Procedure

1. Clean sample with alcohol wipe and let it dry for about 30 minutes.
2. Apply thermocouples at desired locations using the yellow kapton tape (the blue kapton tape detaches as temperatures reach close to 80°C). Note that thermocouple application is a very important step. If not done properly they could detach mid-test.
3. Use a dyneema wire to hang the setup and connect power supply cables.
4. Connect thermocouples to NI 9211 device which in turn is connected to a USB hub inside the vacuum chamber.
5. Seal the vacuum chamber and start the vacuum pump.
6. Once the pressure reaches 0.1mbar, start logging data in LABVIEW.
7. Supply power and wait for steady state to be achieved. This is considered as a maximum change of 1 K/hr plus time constant - show calc from esatan.
8. Turn off power supply and vacuum pump, and then open the valve on the chamber to restore ambient pressure.
9. Remove the test article and clean the area to prepare for the next test.

B.2. Sample Calculation:

$$Power = 0.5W$$

$$T_{\text{heater}} = 45^{\circ}\text{C}$$

$$T_{\text{wire}} = 30^{\circ}\text{C}$$

$$T_{\text{amb}} = 20^{\circ}\text{C}$$

$$A = 0.0016m^2$$

$$Radiation = \epsilon\sigma A(T_{heater}^4 - T_{amb}^4) = 0.2W$$

$$\therefore \text{Heat Loss} = 0.5 - 0.2 = 0.3W$$

$$\frac{kA}{L} = \frac{\text{Heat Loss}}{(T_{heater} - T_{wire})} = 0.02\frac{W}{mK}$$

C

PCB Tests

C.1. Thermal Balance Test Procedure

1. Spray the inside of the enclosure box with Lab IR paint of known emissivity.
2. Make cuts in the enclosure box for cables.
3. Wear gloves and clean the components with distilled water.
4. Attach flexible heater & thermocouples as shown in the figure 3.8a.
5. Place the component in the vacuum chamber and connect power supply cable
6. Place the cardboard enclosure box over setup & remove cables from the cutouts.
7. Ensure power supply voltage is set to zero.
8. Connect thermocouples to NI 9211, which in turn should be connected to the data acquisition computer.
9. Ensure connection to computer is set up and data logging is ready.
10. Seal the vacuum chamber and begin reducing the air pressure inside the chamber and monitor the analog pressure gauge until the required vacuum level is reached. ECSS standards mention 10^{-5} mbar, which is not achievable in the current vacuum chamber so, a value of 0.1 mbar will be used.
11. Set voltage in order to get desired power supply.
12. Monitor temperature sensors and power.
13. Continue the test until the test article reaches steady-state temperature. ECSS standard requires 0.1K/hr over a period of 5 hours. But for our test case scenario, the temperature vs time graph was was visually observed and when the change was less than 0.5K over a period of 10 minutes, steady was assumed to have been acheived.
14. Stop data logging and save data.
15. Stop power supply.
16. Restore ambient pressure.
17. Open the chamber only after ambient pressure is reached.
18. Allow the test article to passively cool to ambient temperature.
19. Store data for analysis.
20. Clean up the work area and ensure the vacuum chamber is ready for the next test.

D

Reduced model results

D.1. 0.488 W

A	**34.3**	35	34.3	**B**	**34.3**	36.3	34.3
	35	**35**	35		36.3	36.6	36.3
	34.3	**35**	34.3		34.3	36.3	34.3
C	31	**31.1**	31	**D**	30	**30**	30
	31.1	**32.4**	31.1		30	30	30
	31	31.1	31		30	30	30

Figure D.1: Experimental results(temperature values in °C) for P_{in} = 0.488 W

A	34.3	35.6		**B**	34.3	36.1	
		36.3				37.8	
C	31.8	31.8		**D**	29.3	29.3	
		31.8				29.3	

Figure D.2: Calculator results(temperature values in °C) for P_{in} = 0.488 W

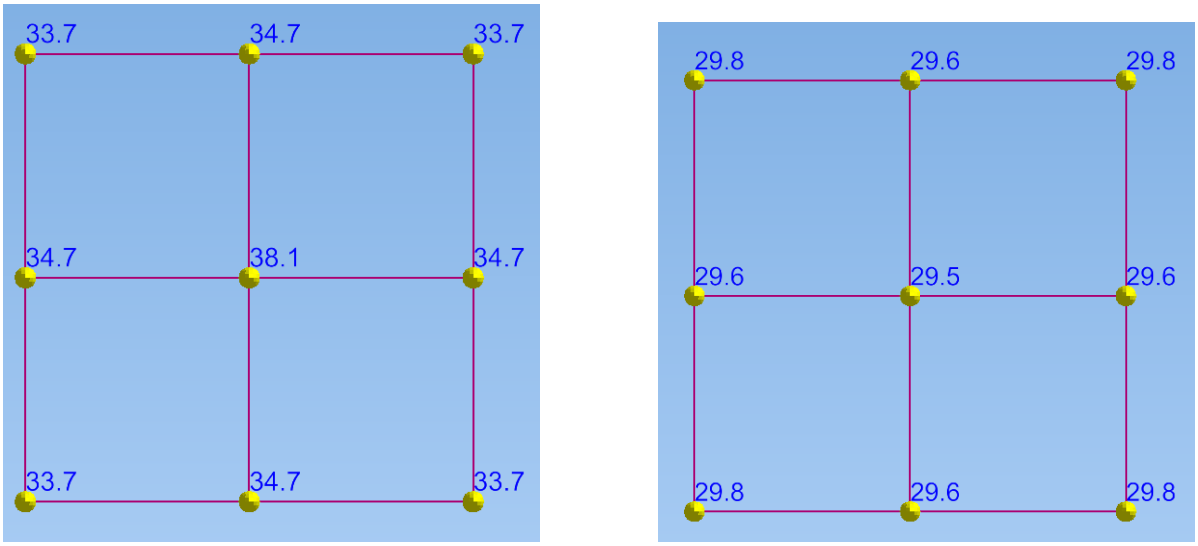

(a) PCB 1 **(b)** PCB 2

Figure D.3: ESATAN results(temperature values in °C) for $P_{\text{in}} = 0.488$ W

D.2. 0.296 W

A	**28**		28	**B**	**28**		28
						32.6	
	28		28		28		28
C	27.3		27.3	**D**			
		28.5					
	27.3		27.3				

Figure D.4: Experimental results(temperature values in °C) for P_{in} = 0.296 W

A	28.7	29.5		**B**	28.7	29.7	
		29.8				30.8	
C	31.8	31.8		**D**	24.5	24.5	
		31.8				24.5	

Figure D.5: Calculator results(temperature values in °C) for P_{in} = 0.296 W

This test was conducted only once, hence thermocouple data obtained only from a few locations. This was done because the temperatures are so close that the available values are enough for discussion.

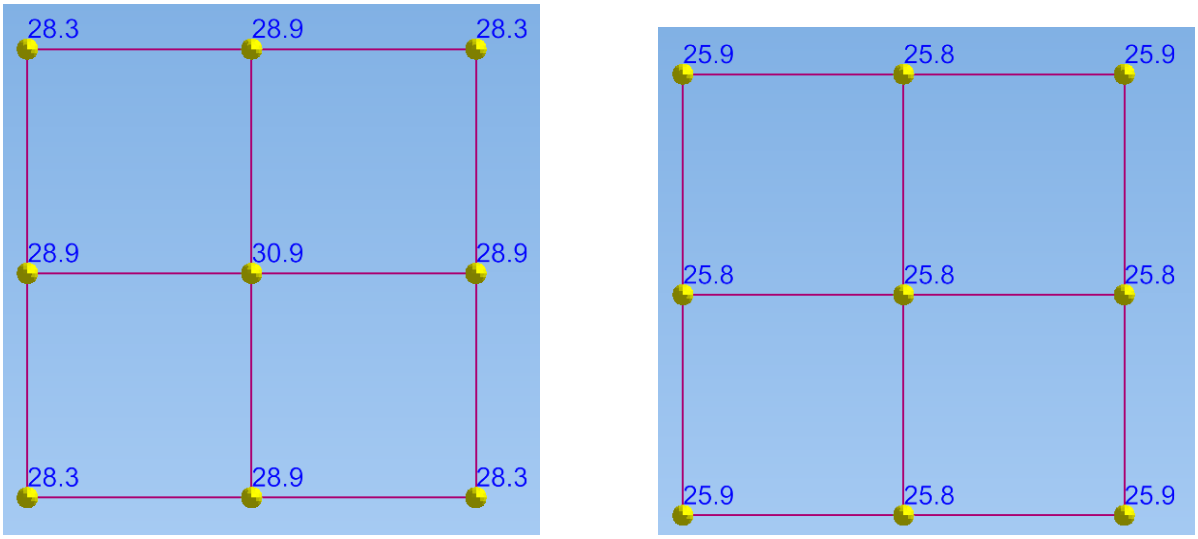

(a) PCB 1

(b) PCB 2

Figure D.6: ESATAN results(temperature values in °C) for $P_{\text{in}} = 0.296$ W

E

Components used in testing

All the components mentioned below are present inside a box in the cleanroom.

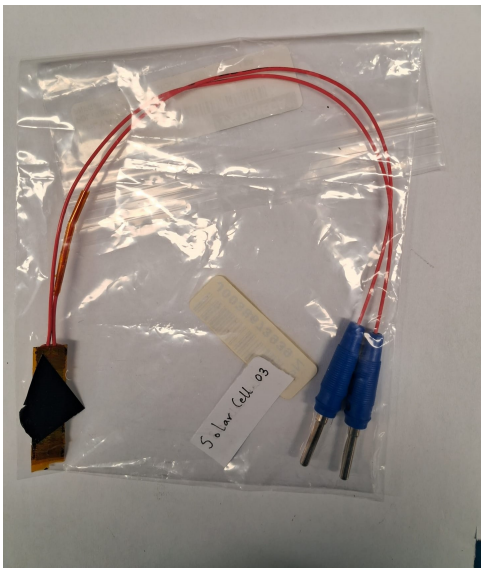

Figure E.1: Solar cell and heater used for solar cell infrared emissivity test

Figure E.2: Solar Panel samples used for solar absorptivity test

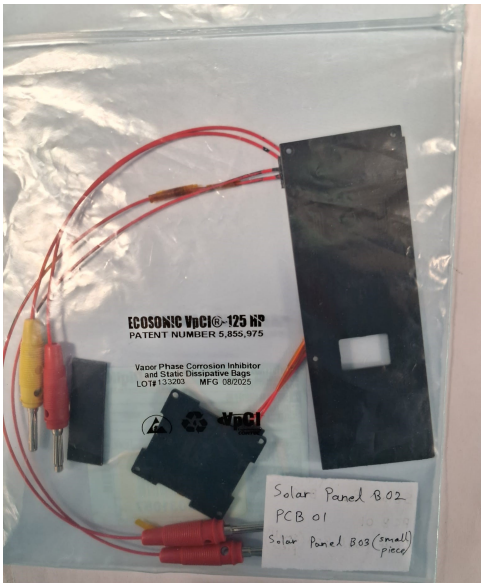

Figure E.3: Samples used for thermal balance tests for heat loss estimation, PCB and solar panel thermo-optical properties

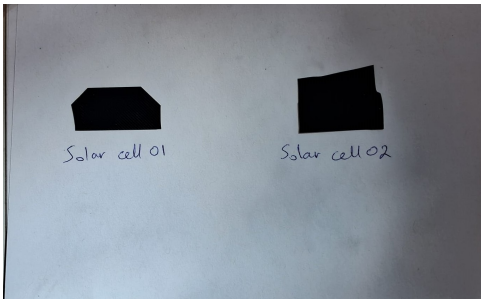

Figure E.4: Solar cells for solar absorptivity measurements

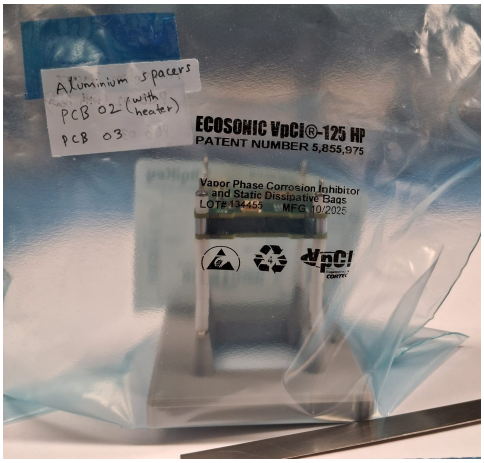

Figure E.5: PCB-stack for linear conductance and reduced model

Symposium Paper

5th Symposium on Space Educational Activities
Munich, April 2026

Improving Thermal Estimates for Student-Built CubeSats

Dhrumil Patadia[1], *Ines Uriol Balbin*[2], *Sevket Uludag*[3], *Stefano Speretta*[3]

Abstract

CubeSats, particularly those developed by student teams, often face extremely short development cycles, leading to limited attention to detailed thermal analysis. Accurate thermal modelling is important to ensure the reliable operation of on-board systems. However, professional thermal modelling tools such as ESATAN are complex, and correlation-based validation methods are time-consuming and resource-intensive. Consequently, small satellite teams frequently rely on simplified models with large error margins in temperature predictions.

This paper presents the design of experiments to determine thermo-optical properties for materials commonly used in student CubeSat construction. Additionally, a database is presented that highlights the thermal conductivity, solar absorptivity, heat capacity and infra-red emissivity, obtained from the experiments, for printed circuit boards (PCBs), solar cells and solar panels. Finally, a sensitivity analysis is performed to indicate the effect of the uncertainties in property values on the average battery temperature as it is a thermally critical component.

The design of experiments can be used by student teams to perform their own experiments and the properties obtained in this work can be used for their initial thermal design. This will allow student teams to make better estimates for the thermal budget of their CubeSat missions.

Keywords
Thermal Testing, ESATAN-TMS, CubeSats, Student Teams

[1] Corresponding author: Delft University of Technology, Netherlands,[2] Aerospace Structures & Materials, Aerospace Engineering, Delft University of Technology, Netherlands

[3] Space Engineering, Aerospace Engineering, Delft University of Technology, Netherlands

Nomenclature

$A(\lambda)$: absorbance (raw data)

C_P: heat capacity

I: intensity measured by sensor

I_o: incident intensity

k: thermal conductivity

$\alpha(\lambda)$: fraction of light absorbed

α_S: effective solar absorptivity

ε_{IR}: infrared emissivity

E_λ: solar spectral irradiance

$r(\lambda)$: fraction of light reflected

Q_{rad}: Radiation heat flow

Abbreviations

PCB: Printed circuit board

IR: Infrared

TC: Thermocouples

TU: Technical University

PQ: pocketcube

1. Introduction

For CubeSats, thermal control is more difficult because they are small, have limited surface area to reject heat, and have low available power for active systems [1][2]. Therefore, their thermal performance depends mainly on good design choices and proper material selection from the beginning. Although advanced software tools such as ESATAN-TMS and Thermal Desktop can perform detailed thermal analysis, they require significant time and experience to use.

SmallSats developed by student teams often give low priority to thermal analysis and design due to lack of funds, development time and experience with thermal analysis software [3].

Guerra et al. [6] also highlight how CubeSats are built using components off the shelf and that thermal control engineering in these projects is overlooked due to the time required and its complexity. Other examples that highlight these issues are student CubeSats such as the ones from Technical University (TU) Delft [4] and TU Darmstadt [5].

The student team at TU Darmstadt could not perform a proper thermal analysis due to software licensing issues and had to rely on a MATLAB code available which imposed certain limitations on the way the configuration can be defined and the lack of attitude modification of the satellite [5].

TU Delft pocketcube (PQ), Delfi-PQ, experienced “unforeseen problems” [4] which led the electrical power sub system to operate from -10°C to 25°C, instead of the planned range of 5°C to 40°C.

While literature provides a reference for thermo-optical values, the sensitivity of CubeSat temperatures to external surface properties, combined with the high variability of thermal properties, results in large observed discrepancies in flight missions such as Delfi-PQ [7].

Therefore, an experimentally validated database of thermo-optical properties for commonly used CubeSat components is necessary. To address these issues, this work aims to determine thermal (k & C_P) and optical (α_S & ε_{IR}) properties for commonly used components like PCBs, solar panels and solar cells used by the student teams at TU Delft. This paper is a part of the ongoing thesis work at TU Delft. The progress made so far has been shared in this paper.

2. Design of Experiments

To measure the thermal and optical properties of the selected components different tests were designed and executed. First, solar absorptivity was measured using a spectrometer (2.1). Secondly, k, ε_{IR} and C_P were measured using thermal balance tests (2.2). Finally, an infrared camera was used to measure the emissivity of the solar cells.

2.1. Solar absorptivity test

Solar absorptivity has been measured using the Lambda 1050 S spectrometer with an integrating sphere. The machine gives raw data of absorbance for each wavelength which must be converted into the effective solar absorptance of the sample. The procedure is shown below.

$$A(\lambda) = -log_{10}(\frac{I}{I_o}) \qquad (1)$$

The ratio $\frac{I}{I_o}$ represents the reflection ratio, r

$$A(\lambda) = -log_{10}(r(\lambda)) \qquad (2)$$

$$r(\lambda) = 10^{-A(\lambda)} \qquad (3)$$

$$\alpha(\lambda) = 1 - r(\lambda) = 1 - 10^{-A(\lambda)} \quad (4)$$

The effective solar absorptivity is then calculated as

$$\alpha_S = \frac{\Sigma\, \alpha(\lambda) * E_\lambda}{\Sigma E_\lambda} \quad (5)$$

E_λ can be obtained from the work done by Gueymard [8].

This test was done for solar cells, green, white and black solar panels having dimensions of approximately 30mm × 30mm.

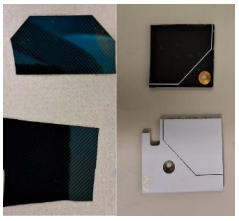

Figure 1. Solar Cell and Solar Panel

2.2. *Thermal Balance tests*

Thermal balance tests, inside the vacuum chamber, have been performed for the determination of thermal conductivity, heat capacity and infrared emissivity. For these tests, heat is provided using a tape heater and temperatures along the surface of the sample are measured using thermocouples. It is important to account for heat loss from heater. The heat loss calculations have been shown in the Appendix.

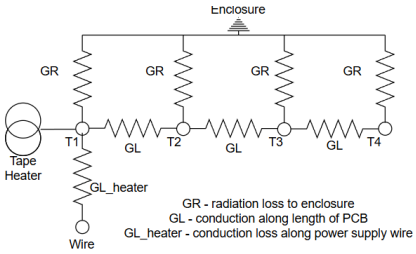

Figure 2. Thermal network – PCB

This thermal network represents the thermal balance test set-up as shown in Figure *3*.

The test was carried out inside a vacuum chamber, and the setup was enclosed by a box (shown in *Figure 3*) whose surface had a known emissivity ($\varepsilon_{IR} = 0.8$) to account for the radiative exchange factor. During this test, 0.5W of power was supplied to the heater and the steady state temperatures of the samples were recorded.

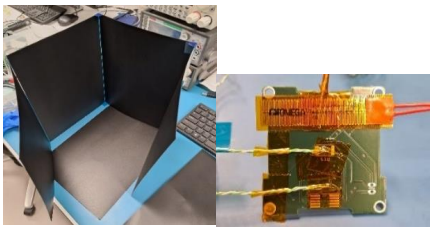

Figure 3. Enclosure ($\varepsilon_{IR} = 0.8$) and PCB Test 1 setup

For representation purposes, the thermal network (*Figure 2*) considers the PCB to be divided into 4 elements. For this thermal balance test, referred to as **Test 1**, during the steady state heat flows through three paths: Heat loss from heater, Conduction along the length of PCB, and Radiation from the surface of the PCB

Of these three paths for the heat flow, two of them: the radiation and conduction of the sample are unknown. This makes the steady state heat balance equation unsolvable as there are two unknowns.

To solve this problem, another thermal balance test was conducted for the same setup, say, **Test 2**. The only difference between both tests was that test **1** was with a bare PCB, while test **2** was with the paint ($\varepsilon_{IR} = 0.8$) coated PCB. This meant that the only unknown in test 2 was the thermal conductivity.

Now, the steady state thermal balance equation for this can be used to determine this thermal conductivity. Further, this value from **Test 2** can be fed to the data obtained from **Test 1** to determine the infrared emissivity of the PCB.

Figure 4. PCB with LabIR paint of known emissivity (ε_{IR} = 0.8) for Test 2

Finally, for determination of the heat capacity (C_P), the heater was turned off at the end of steady state and the time taken for the PCB to

reach back to room temperature was recorded. A code was written to model this transient phase which gave the heat capacity of the sample.

The exact same procedure has been followed to determine properties of the black solar panel. The green and the white solar panel are considered to have the same thermal properties as only the surface paint varies amongst them.

For all these tests, the error sources have been identified and uncertainties in measurements have been propagated from TC accuracy (±2.2K), paint emissivity (±0.013), length and power supply measurements

2.3. *Test with Infrared camera*

This test includes a solar cell sample attached to a tape heater whose temperature was measured using a thermocouple (*Figure 5*).

Figure 5. Solar cell test setup for IR camera measurement

By changing the power given to the sample via the heater two different temperature states were considered. At both power levels, the temperature is measured both via the infrared camera as well as the thermocouple. The only constant is the surrounding radiation reflected by the solar cell. With these data the infrared emissivity of the sample can be calculated assuming it is constant at both temperatures.

3. Results and Discussion

Table 1. Database of properties

Sample	α_S	ε_{IR}	k	C_P
Solar cell (A)	0.90	0.93	-	-
Solar cell (B)	0.834	0.93	-	-
PCB	-	0.84	10	550
Black solar panel	0.77	0.92	25	660
White solar panel	0.33	-	25	660
Green solar panel	0.32	-	25	660

In the above table, the unit of k is $Wm^{-1}K^{-1}$ and Cp is $Jkg^{-1}K^{-1}$

The table above gives the nominal values of properties. The further discussion will highlight the uncertainty in the values obtained.

3.1. *Solar absorptivity*

The measured values of solar absorptivity and the reference values that were used in previous CubeSats developed by TU Delft are shown in *Table 2*. Looking at the values obtained for the solar cells and the black solar panel (used in Delfi-PQ), they are lower than the reference value. This is one of the factors that could have contributed to Delfi-PQ experiencing a lower temperature than expected as discussed in the introduction.

Another important aspect to note is the variation in the solar absorptivity of the white solar panel. Nasa [15] highlights that white coatings can have a wide range of values for solar absorptivity from 0.17 to 0.39. Thus, it is important to measure the value, if white solar panels are being used, as manufacturers would usually not provide this value.

Table 2. Solar absorptivity values

Component	Measured α_S	Reference	Variation
Solar cell	0.902 (Sample A)	<0.91 [9]	0.8%
	0.834 (Sample B)		8.4%
Black Solar Panel	0.867	0.94 [10]	7.8%
White Solar panel	0.331	0.21 [10]	57%
Green Solar Panel	0.324	-	

3.2. *PCB properties*

The measurements made for the PCB and the reference values found in literature are shown in Table 3.

Table 3. PCB measured properties

Property	Measured Value	Reference Value
k ($Wm^{-1}K^{-1}$)	10 ± 5	17.7 [12]
C_P ($Jkg^{-1}K^{-1}$)	550 ± 40	589 [7]
ε_{IR} (-)	0.86 ± 0.06	0.8 to 0.91 [13]

The measured thermal conductivity is approximately 40% lower than the value commonly reported in the literature. A comparison with additional literature sources [14] also indicates that the obtained value is lower than expected. The error could be due to multiple reasons: error in heat loss estimation or heat leak through thermocouple cables. The

experiment was repeated, and similar temperature distributions were observed, suggesting that the deviation is likely not due to random measurement error. Instead, it may indicate a lower copper content in the tested PCB than assumed which can differ between suppliers and even between production batches from the same supplier.

The source of uncertainty stems from the variability of heat loss and thermocouple accuracy of ±2.2K.

3.3. Solar panel properties

The measurements made for the solar panel are shown in *Table 4*.

Table 4. Solar Panel measured properties

Property	Measured Value	Reference Value
k ($Wm^{-1}K^{-1}$)	25 ± 15	34 [12]
C_P ($Jkg^{-1}K^{-1}$)	660 ± 130	575 [7]
ε_{IR} (-)	0.92 ± 0.03	Close to unity [10]

The solar panel used has a copper content around 2 times that of the PCB, thus a value of thermal conductivity close to 25 W/mK is justifiable.

3.4. Solar cell properties

The solar cell is adhesively attached to the solar panel, and it is very thin and light compared to the panel, thus its thermal conductivity and heat capacity will not be considered. But it covers a major portion in terms of area of the solar panel, thus its solar absorptivity and infrared emissivity are of utmost importance.

Property	Measured Value	Reference Value
ε_{IR} (-)	0.93 ± 0.07	Close to unity [10]

The measurements from the thermal camera had high uncertainty and this led to an emissivity range between 0.86 and 1 which makes the results not useful. This is because of the accuracy of TC (±2.2K) and camera(±3K).

4. Sensitivity Analysis

The experimentally obtained properties were used in the thermal model of Delfi-PQ, and their uncertainties were applied as bounds to determine temperature sensitivities.

One-at-a-time sensitivity analysis was carried with the parameters listed in *Table 5* and the average battery temperature, being a thermally critical component, was observed.

Table 5. Properties for Sensitivity Analysis

Component	Property	Value
PCB	C_P ($Jkg^{-1}K^{-1}$)	550 ± 40
	ε_{IR} (-)	0.86 ± 0.06
Solar Panel	C_P ($Jkg^{-1}K^{-1}$)	660 ± 130
	ε_{IR} (-)	0.9 ± 0.1
	α_S (-)	0.77 ± 0.1
Solar Cell	ε_{IR} (-)	0.93 ± 0.07
	α_S (-)	0.61* ± 0.03

* Considering 30 % solar cell efficiency

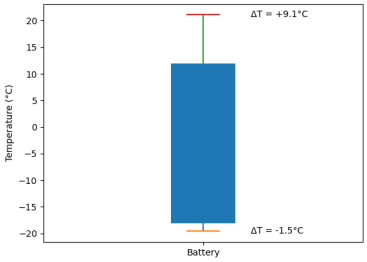

Figure 6. Battery temperature deviation due to uncertainties in properties

The blue boxplot indicates the average temperature of the battery if nominal values of properties mentioned in *Table 5* are used. The deviations on either side of +9.1°C and -1.5°C arise due to uncertainties in properties. Thus, student teams should account for these in their thermal models when considering the nominal working temperatures usually given by manufacturers.

5. Future work and conclusions

This study experimentally determined thermo-optical and thermal properties for PCB and solar panel components commonly used in student-built CubeSats. Solar absorptivity measurements showed deviations of up to 7–8% compared to reference values previously adopted in CubeSat thermal models. More significantly, the measured thermal conductivity of the PCB was approximately 40% lower than commonly cited literature values. Although measurement uncertainties exist, repeated experiments produced consistent temperature distributions, indicating that the deviation is likely linked to material composition variability, such as copper content or supplier-dependent FR4 properties.

These results highlight the risk of directly adopting literature values for preliminary thermal modelling without validation.

The experimental approach presented here demonstrates a practical method for student teams to obtain more representative material properties using accessible laboratory equipment.

The next phase of the research will focus on development of reduced-order thermal models.

Appendix

For the determination of heat loss, the heater was attached to a piece of solar panel having the same dimensions as the heater. Both the heater and the solar panel were covered with LabIR paint [11] to ensure a known emissivity ($\varepsilon_{IR} = 0.8$). The test was conducted at a pressure of 0.12mbar (lowest achievable in the vacuum chamber available).

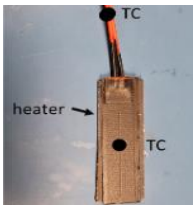

Figure 7. Heat loss estimation test setup

Table 6. Heat loss estimation

Power Input	Heater Temp.	Wire Temp.	Q_{rad}	Heat loss
0.5W	45°C	30°C	0.2W	0.3W
1.5W	92°C	40°C	0.74W	0.76W

This heat loss data gives an effective heat loss coefficient of 0.015 ± 0.006 WK^{-1}.

References

[1] European Cooperation for Space Standardization, *ECSS-E-ST-31C: Space engineering – Thermal control general requirements*, 15 Nov. 2008.

[2] National Aeronautics and Space Administration, “7.0 Thermal control,” in *State-of-the-Art Small Spacecraft Technology Report 2024 Edition*, Feb. 5, 2025.

[3] A. Alanazi and J. Straub, “Engineering methodology for student-driven CubeSats,” Aerospace, vol. 6, 5 2019.

[4] Z. Zhang and S. Speretta, “Orbital Temperature Model Construction for Delfi-PQ,” TU Delft, technical report.

[5] J. Gomez, “Thermal Analysis, Design and Verification of an Academic CubeSat Mission in a MBSE Context,”, master thesis, TU Darmstadt, 2024.

[6] A. G. C. Guerra, D. Nodar-Lopez, and R. Pardavila, “Thermal analysis of the electronics of a CubeSat mission,” arXiv, 2018.

[7] R. ´Avila De Luis, “Standardized Thermal Control Solutions for Pocketcubes,” TU Delft, 2019

[8] C. A. Gueymard, “Revised composite extraterrestrial spectrum based on recent solar irradiance observations,” Solar Energy, vol. 169, pp. 434–440, 7 2018.

[9] “Azur Space: Triple Junction GaAs Solar Cell,”,https://www.azurspace.com/media/uploads/file_links/file/bdb_00010891-01-00_tj3g30-advanced_4x8.pdf, last visited: 28-02-2026.

[10] V. N. Gorev, et al. “The effect of the PCB solder mask type of the hull outer surface of the CubeSat 3U on its thermal regime,” IOP, 2020

[11] LabIR Paints, https://paints.labir.cz/en/paints/herp-ht/, last visited: 28-02-2026.

[12] K. Azar and J. E. Graebner, “Experimental determination of thermal conductivity of printed wiring boards,” Annual IEEE Semiconductor Thermal Measurement and Management Symposium, pp. 169–182, 1996.

[13] M. M. Finckenor and R. F. Coker, “Optical Properties of Nanosatellite Hardware,” NASA NTRS, 2014.

[14] A. K. Te Nijenhuis, et al., “Thermal Analysis and Verification of CubeSat Designs with ESATAN-TMS,” in 50th ICES, vol. 104, pp. 12–15, 2021

[15] L. Kauder, “Spacecraft Thermal Control Coatings References,” Technology Report, NASA, 2005.